WIICT2022

Proceedings of the Workshop on Innovation on Information and Communication Technologies 2022

Institute ITACA
Information and Communication Technologies

Editors:
Dr. Carlos Fernandez-Llatas
Dra. Maria Guillen

Committees

Organizing Committee

- **Chair**:Maria Guillem, Universitat Politècnica de València, Spain
- Alberto Bonastre, Universitat Politècnica de València, Spain
- Jose Manuel Catala, Universitat Politècnica de València, Spain
- Carlos Fernández-Llatas, Universitat Politècnica de València, Spain
- Jose Mariano Dahoui, Universitat Politècnica de València, Spain

Scientific Committee

- **Chair**: Carlos Fernandez-Llatas, Universitat Politècnica de València, Spain
- Paulo de Carvalho, University of Coimbra, Portugal
- Anna-Maria Bianchi, Politecnico di Milano, Italy
- Jorge Munoz-Gama, Pontificia Universidad Catolica de Chile
- Fernando Seoane, Karolinska Institutet
- Jorge Henriques, University of Coimbra, Portugal
- Cenk Demiroglu, Ozyegin University, Turkey
- Johan Gustav Bellika, National Center of Telemedicine, Norway
- Yigzaw Kassaye Yitbarek, University of Tromso, Norway
- Raymundo Barrales, Universidad Autónoma Metropolitana de México
- Onur Dogan, Istanbul Technical University,, Turkey
- Frank Y. Li, University of Agder, Norway
- Pilar Sala, MySphera., Spain
- Alvaro Martinez, MySphera, Spain
- Jose Carlos Campelo, Universitat Politècnica de València, Spain
- Juan Vicente Capella, Universitat Politècnica de València, Spain
- Antonio Mocholí, Universitat Politècnica de València, Spain
- Sara Blanc, Universitat Politècnica de València, Spain
- Juan-Carlos Baraza-Calvo, Universitat Politècnica de València, Spain
- Juan Carlos Ruiz, Universitat Politècnica de València, Spain
- Joaquin Gracia, Universitat Politècnica de València, Spain
- David De Andres, Universitat Politècnica de València, Spain
- Ricardo Mercado, Universitat Politècnica de València, Spain
- Alejandro Liberos, Universitat Politècnica de València, Spain
- Lenin Lemus, Universitat Politècnica de València, Spain
- Vicente Traver, Universitat Politècnica de València, Spain
- Antonio Martinez-Millana, Universitat Politècnica de València, Spain
- Jose Luis Bayo-Monton, Universitat Politècnica de València, Spain
- Juan Miguel García-Gomez, Universitat Politècnica de València, Spain
- Elies Fuster, Universitat Politècnica de València, Spain
- Carlos Saez, Universitat Politècnica de València, Spain
- Ángel Perles, Universitat Politècnica de València, Spain
- Luis José Saiz Adalid, Universitat Politècnica de València, Spain
- Gema Ibañez, Universitat Politècnica de València, Spain
- Pedro Yuste, Universitat Politècnica de València, Spain
- Daniel Gil Tomàs, Universitat Politècnica de València, Spain
- Sabina Asensio, Universitat Politècnica de València, Spain
- Beatriz Garcia-Baños, Universitat Politècnica de València, Spain
- Francisco Castells, Universitat Politècnica de València, Spain
- Diogo Nunes, University of Coimbra, Portugal
- Adriana Leal, University of Coimbra, Portugal
- Zoe Valero Ramón, Universitat Politècnica de València, Spain
- Yolanda Vives, Universitat Politècnica de València, Spain

- Victoria Lerma, Universitat Politècnica de València, Spain
- Edgar Lorenzo, Universitat Politècnica de València, Spain

Table of Contents

Knowledge-based change management methodology for healthcare organizations

Gema Ibanez-Sanchez[1], Carlos Fernandez-Llatas[1,3], and Martin R. Wolf[2]

[1] SABIEN-ITACA Universitat Politècnica de València, geibsan@itaca.upv.es, cfllatas@itaca.upv.es
[2] Faculty of Electrical Engineering and Information Technology FH, Aachen University of Applied Sciences, m.wolf@fh-aachen.de
[3] Department of Clinical Science, Intervention and Technology (CLINTEC) Karolinska Institutet, Stockholm, Sweden
carlos.fernandezllatas@ki.se

Abstract. Adopting digital tools in health organizations is a long journey plenty of obstacles. This paper proposes a methodology to generate a changing culture in healthcare organizations using a supportive software solution like Interactive Process Mining, which incorporates new team-based and knowledge-based approaches for continuous quality of care improvement.

Keywords: Methodology; change culture; lean thinking; interactive process mining; objective data; high-value care

1 Introduction

The life expectancy of the world's population is increasing vertiginously, accompanied by challenges that directly impact the health systems around the world[3]. Optimizing health care to improve or maintain health at a time that responds to changing population necessities is needed for their sustainability and the provision of good health care. In this line, different initiatives propose to estimate the impact of health systems on patients' health, user experience, and economic benefits by developing mechanisms to measure and use data to learn where improvements are needed and to track the value of the health system [14, 8, 17]. Different macro, meso and micro-level strategies are suitable for tackling political, economic, or organizational aspects of health systems. This improvement goes through having a learning system with accurate and timely data and a health system leadership committed to improving data literacy for health workers, being micro-level interventions mainly focus on directly influencing staff performance and protocols to enhance the quality of care, needing a detailed measurement of the patient journey and context data[8].

New technologies are a key piece of the puzzle to support measuring value for patients and to help on the way towards a paradigm change of the health systems[18, 12]. In this regard, Big data is one of the most promising technologies, however, in some cases acts as *black boxes*, a known effect that does not explain where comes from the results are obtained, preventing health experts from trusting these systems. It is paramount to ensure transparency in all aspects of these technologies since their use can negatively impact patients' health. Consequently,

C.Fernandez-Llatas and M.Guillen (Ed.):
Workshop on Innovation on
Information and Communication Technologies
(ITACA-WIICT 2022)

ISBN 978-84-09-46075-5

appropriate tools and methodologies are needed to support health experts and hospital staff in enhancing the health system.
Nonetheless, it implies a radical change in the mindset of health professionals, in their data value culture[12], and the coordination among teams that usually take long[10, 6], resulting in resistance [20], which is one of the main barriers associated with the digital health transformation[11, 1].
Our proposal to deal with this is a knowledge-based change management methodology (Figure 1) to foster the adoption of digital solutions to contribute to a transformation toward high-value care-based health systems.

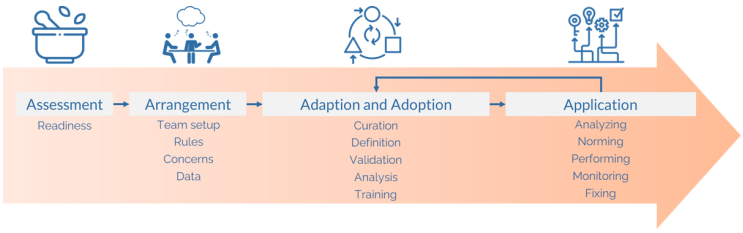

Fig. 1. Interactive Process Mining-informed change management methodology for healthcare

2 Materials and methods

These barriers can be softened by working at different levels in the organizations. Change management techniques and the selection of appropriate technology can contribute to this purpose of preparing individuals and organizations to adopt changes successfully [7, 15]. In this regard, Interactive Process Mining (IPM)[4] is proposed since it offers medical experts a direct understanding of the results by allowing them to navigate the different layers of information to find answers to posed questions and apply their experience and knowledge to the improvement process. Interactive Process Mining is able to measure changes objectively, before, during and after any modification, providing to the experts information about evolution, outcomes and associated issues[4]. IPM is a paradigm where multidisciplinary teams, usually composed of an expert on Process Mining (**Process Miner**) and at least one health professional (nurses, doctors...) per field analyzed (i.e. emergency department, laboratory...), are participating on iterative co-creation sessions (known as **Data Rodeos**). The objective of these Data Rodeos is to define an **Interactive Process Indicator** (IPI), which can be seen as a kind of ameliorated Key Performance Indicator (KPI). IPIs are focused on depicting a process, taking it as the central element for the analysis. Furthermore, KPIs can be part of the IPI to navigate into them as well as statistics and other functionalities that allow going into detail inside the data. Data rodeos aim to understand the data, deal with data quality, define and analyze the IPI when health professionals are taught to use the tool and provide them with process analysis skills.
On the other hand, the literature presents us with various theories to manage changes. *Kubler*[9] presented a work showing the phases of a change from a

psychodynamic point of view, where an individual went through shock, denial, frustration, depression, experiment, decision and integration until acceptance. This theory focused efforts on modifying the behavior of individuals, who are at the center of every change in organizations, highlighting the importance that once individuals are motivated, the organization is ready to materialize a change. Also, it is necessary to consider that individuals are ruled by organization policies, belong to teams and interact among them, being an individual, team and organizational aspects enabling a framework for this change management. Concerning this, Cameron at al[2] proposed five areas to conduct a smoothly change at the team level, which were 1) nature of the change, 2) persons who benefit from the change, 3) organizations that handle the change (culture); 4) types of the personality of each individual, and 5) previous individual experience. Even though change management not only takes care of managing teams, it is also that the team should be effective in their actions, for what aspects such as defining a team goal and a plan for it, identifying roles, procedures, interpersonal relationships, and inter-team relations at the organizational level are crucial to success[2, 13]. Another critical element is the identification of the type of organization and how it works[16, 5], but most are the non-written rules behind the organization that influence highly in the change process [19].
Acceptance is influenced by a person's behavior, their personality, and the context in which it is located. It is necessary to facilitate the conditions to gain the best possible acceptance. However, if people lack the right mindset to change and organizations do not set strategies to manage and embrace it, they will not success[21]. The individual, team and organizational aspects of the changes should be integrated into a coherent whole, enabling a framework for this change management.

3 Results

Based on the theories introduced in the previous section, Interactive Process Mining-Induced Change Management Methodology for healthcare is presented. It is thought to support adopting IPM technology for transforming health organizations. The core team behind the methodology is mainly composed of an expert guiding the change **link manager**, who works with the **Interactive Process Miner**, in charge of dealing with IPM. This team can also include communication or training managers. **IT professionals** and **health professionals** (managers, directors, heads of unit, clinicians, which can be doctors, nurses...) are needed from the health organization side. They complete the multidisciplinary team to carry out the co-creation data rodeo sessions and the transformation process.

3.1 Assessment

It is the first contact with the organization, where the link manager needs to assess the readiness of the organization to embrace the change. In this phase, essential aspects are presenting the working strategy to the management team to get their support, additional time for the group participating from the hospital, and rewards to motivate them. Also, to conduct informal meetings to understand tasks formally defined and the unwritten activities to understand the political map of the organization as well as identify who will resist or foster the change. As a result, a **readiness assessment** is obtained on aspects such as the *management team*

(management agrees on new changes and actively supports them), *target definition* (targets are clearly defined, communicated and accepted in the organization), *performance of the organization* (performance indicators of the health organization), *processes* (the extent processes and standardized proceedings are defined and followed), *dissatisfaction* (of the medical staff current situation), *communication* (the extent relevant information is shared within the health organization) and *people involvement* (medical teams are voluntarily involved in decisions of the health organization) and a **stakeholders' Map**, where can be identified people resistant, neutral, that accept the change, are supportive or really committed.

3.2 Arrangement

When the link manager knows the organization, a workshop to prepare the organization for the change is organized in five stages. Health professionals can attend the workshop voluntarily, taking no more than a morning day.

1. **Team setup**. Participants are welcomed with some snacks to create a comfortable atmosphere to work. They introduce themselves and the conductors of the change: who they are (name, position, technology literacy), what they do and why they are there (motivation).
2. **Orientation and creativity**. It helps to understand the process, the data needed to build an IPI and the potential problems. Tools such as the patient journey map describe the steps the patient follows when arriving at the hospital or being treated for a specific disease.
3. **Optimization**. This stage aims to identify weak points in the process and prioritize posed questions to be solved, considering project constraints, the complexity around requirements, and available resources (time, costs, and employees).
4. ***Mise en place***. A crucial stage to drive a cultural change in a health organization is the presentation of a schedule. It clearly states the rules for what, why, who, how and when things should be done. The main points that should consider are *1. Vision and Mission* what is the purpose, *2. Sponsors* who is paying, *3. Authorities* who are approving the change, *4. Core* who is managing the change, *5. Team* who is required from the hospital in the change. At this point, champions are introduced as a key element to facilitate the change by assessing how things are going on and identifying what needs to be done, *6. Participants* who can join the change process. *7. Communication*. A communication plan is presented to tackle requests of employees, motivate and manage conflicts employing periodic updates, consultation schedule, channels, contact persons, meetings plan and feedback management. *8. Training*. A training plan is presented with a minimum set of rules that should be established to keep the team motivated to participate. Additional time or equipment and champions supporting the trainers are, in most cases, good leverages to contribute to this point. *9. Rewards*. Reinforcement strategies are one of the most effective motivations. It can be financial and non-financial reinforcements, for example, in the form of feedback. *10. Indicators*. These are derived from the posed questions to be solved.
5. **First contact**. The final step of the workshop is the first contact with IPM to show health professionals how they can analyze their data and get insights as well as other aspects such as ethical issues, data exchange or type of data recommended for the analysis.

3.3 Adaption and Adoption

The proposed methodology aims to break with barriers and resistance at the time to adopting new technology in a health organization. So far, we have been knowing the organization and setting the rules to execute the change, where some improvements are selected to introduce the technology with a profit result. At this stage, the *core* and the *team* work together during the data rodeo sessions to curate data, define, validate and analyze the IPI and train the health professionals or any other profile belonging to the team. Here is also important to gather feedback about the tool in terms of usefulness and user-friendliness.

3.4 Application

Once the IPI is defined, the team can analyze it and start with the application phase, where analysis in more detail is done as well as modifications in the organization to achieve the aim of improving the value offered to patients. Furthermore, since the fundamental of the IPIs is process-based analysis, this can contribute not only to the analysis but also in:

- understanding each step of the process
- identifying where there are problems such as bottlenecks, delays, rework, and other forms of waste
- identifying where the root causes are
- orienting new staff in the process
- describing clearly the process to other departments

This phase is composed of five stages: **1) analyzing**, a deeper analysis is done until finding root causes and answers to questions that contribute to improving the functioning of the organization, **2) norming**, the objective of the previous phases were to introduce IPM in the organization and teach the health professionals in its adoption through an example that bring them to a real improvement in the organization. Instead, in the *Application* stage, this learning process is finalizing, and it is needed to define the rules for continuing this work by themselves. Then, the objective in the *norming* stage is to define a set of rules (similar to the *Arrangement* phase) to understand how the use of IPM will work once the *core* team leaves and the *team* incorporate the use of IPM in their daily practice. They need to know what will be the objective of using IPM (*Vision and Mission*), the *team*, making special emphasis on the roles and accountability of each component, and the *communication* rules, which include the dynamic of the team in terms of activities, meetings, communication channels, and feedback (in and out of the team). Here is also necessary to define available *resources* (time and equipment), *rewards* as additional payment for the effort on improving the organization, *training* will be required to teach about new ways of working, and *indicators* to identify measurements to compare the evolution (favorable or not). The following stages are **3) performing**, where in those more complex cases that the necessity is identified, the *core* team will include a *continuous improvement manager* to look for more concrete enhancements, **4) monitoring**, this stage measures the technology acceptance of IPM solution as well as the establish a baseline to compare the results during and after modifications, and finally **5) fixing**, after introducing IPM in the health organization and producing a prosperous enhancement in the organization. This stage is in charge of establishing a new beginning with a party.

4 Conclusions

The sustainability of the health systems goes through a paradigm change where health systems look to improve the population's health through better care and optimizing the available resources. This improvement contributes to reducing costs and inefficiencies that are reflected in the outcomes and expenses. But this paradigm shift is not trivial and needs the support of the new technologies in searching for what and where issues and root causes are in a timely way. IPM offers an agile and transparent technology that allows health professionals to identify and understand their reality. Since any change generates resistance in an organization, it is needed to be treated to minimize its impact. This work proposes a methodology to address the first change in this long path, the mindset change and adopting a disruptive technology toward better health systems.

References

1. David A Buchanan, Louise Fitzgerald, and Diane Ketley. *The sustainability and spread of organizational change: modernizing healthcare*. Routledge, 2006.
2. Esther Cameron and Mike Green. *Making sense of change management: A complete guide to the models, tools and techniques of organizational change*. Kogan Page Publishers, 2019.
3. Kaare Christensen, Gabriele Doblhammer, Roland Rau, and James W Vaupel. Ageing populations: the challenges ahead. *The lancet*, 374(9696):1196–1208, 2009.
4. Carlos Fernandez-Llatas. *Interactive process mining in healthcare*. Springer, 2021.
5. Roger Gill. Change management–or change leadership? *Journal of change management*, 3(4):307–318, 2002.
6. Michelle Halligan and Aleksandra Zecevic. Safety culture in healthcare: a review of concepts, dimensions, measures and progress. *BMJ quality & safety*, 20(4):338–343, 2011.
7. John Hayes. *The theory and practice of change management*. Palgrave, 2018.
8. Margaret E Kruk, Anna D Gage, Catherine Arsenault, Keely Jordan, Hannah H Leslie, Sanam Roder-DeWan, Olusoji Adeyi, Pierre Barker, Bernadette Daelmans, Svetlana V Doubova, et al. High-quality health systems in the sustainable development goals era: time for a revolution. *The Lancet global health*, 6(11):e1196–e1252, 2018.
9. Elisabeth Kübler-Ross, Stanford Wessler, and Louis V Avioli. On death and dying. *Jama*, 221(2):174–179, 1972.
10. L Leape, D Berwick, C Clancy, J Conway, P Gluck, James Guest, David Lawrence, J Morath, D O'Leary, Paul O'Neill, et al. Transforming healthcare: a safety imperative. *BMJ Quality & Safety*, 18(6):424–428, 2009.
11. Maria Lluch. Healthcare professionals' organisational barriers to health information technologies—a literature review. *International journal of medical informatics*, 80(12):849–862, 2011.
12. H Gilbert Miller and Peter Mork. From data to decisions: a value chain for big data. *It Professional*, 15(1):57–59, 2013.

13. Isabel Briggs Myers. *The Myers-Briggs Type Indicator: Manual*. Consulting Psychologists Press, 1962.
14. World Health Organization. *The world health report 2000: health systems: improving performance*. World Health Organization, 2000.
15. Robert A Paton and James McCalman. *Change management: A guide to effective implementation*. Sage, 2008.
16. Paul E Plsek and Tim Wilson. Complexity, leadership, and management in healthcare organisations. *Bmj*, 323(7315):746–749, 2001.
17. Michael E. Porter. What is value in health care? *The New England Journal of Medicine*, 363(26):2477–2481, December 2010.
18. Wullianallur Raghupathi and Viju Raghupathi. Big data analytics in healthcare: promise and potential. *Health information science and systems*, 2(1):3, 2014.
19. Charles R Schwenk. Linking cognitive, organizational and political factors in explaining strategic change. *Journal of Management Studies*, 26(2):177–187, 1989.
20. Dianne Waddell and Amrik S Sohal. Resistance: a constructive tool for change management. *Management decision*, 36(8):543–548, 1998.
21. Bryan J Weiner. A theory of organizational readiness for change. *Implementation science*, 4(1):67, 2009.

Analysis of overheads caused by adding Error Correction Codes in Embedded Systems*

Joaquín Gracia-Morán[1], P. Martín-Tabares[2], C. Martínez-Ruiz[2], Luis J. Saiz-Adalid[1]

[1] Instituto ITACA, Universitat Politècncia de València
Camino de Vera, s/n, 46022 Valencia, Spain
{jgracia, ljsaiz} @ itaca.upv.es

[2] Instituto ITACA, Escuela Técnica Superior de Ingeniería Industrial
Camino de Vera, s/n, 46022 Valencia, Spain
{pabmarta, carma37c} @ etsii.upv.es

Abstract. Nowadays, CMOS technology integration scale has allowed memory systems with a large storage capacity. However, it has also caused an increase in its fault rate.
One possible solution is the use of Error Correction Codes (ECCs). New ECCs are continually being proposed. These proposals consider a multitude of factors, such as redundancy, or different overheads introduced by the ECCs. However, these ECCs are typically designed for large memory systems, whereas few studies have been done analyzing how affects the inclusion of an ECC in an Embedded System. In this work, we have examined how the insertion of a series of ECCs in an Embedded System affects it.

1 Introduction

The increase in the CMOS technology integration scale has allowed the design of memory systems with a large storage capacity, but at the cost of incrementing their fault rate [1]. Thus, the impact of a cosmic radiation particle can cause a bit-flip in one or more memory bits [2], [3], [4].

Usually, SEC (Single Error Correction) codes, able to correct an error in a single bit, or SEC-DEC (Single Error Correction - Double Error Detection) codes, capable of correcting an error in a bit, as well as detecting two errors in two independent bits, are used to protect memories [5], [6], [7]. As fault probability increases, fault coverage of ECCs must also grow, as it happens when ECCs are used in critical applications [8], [9], [10], [11].

As some redundant bits are added to each memory word, usually, the design of an ECC tries to minimize this number of redundant bits. Another aspect to consider is that encoders and decoders introduce some overheads, such as silicon area and power consumption, as well as encoding and decoding latencies.

* Grant PID2020-120271RB-I00 funded by MCIN/AEI/10.13039/501100011033.

C.Fernandez-Llatas and M.Guillen (Ed.):
Workshop on Innovation on
Information and Communication Technologies
(ITACA-WIICT 2022)

ISBN 978-84-09-46075-5

Usually, an ECC is included in a system at design time. So, what happens if we want to include an ECC in an already built system? And, if this system is an Embedded System, is it possible to include an ECC?

Embedded Systems have special properties, such as low memory capacity or low power consumption. As far as we know, there currently exists on the market a fault-tolerant processor specifically designed for embedded systems [12]. In any case, there are few analyses of the impact of the inclusion of an ECC in an embedded system

In this work, and by building a small meteorological monitoring system [13], [14], [15], we have accomplished this type of study. Hence, we have calculated the size of the software and tested whether the software can be executed on time after adding diverse ECCs with different fault tolerance properties. In this way, we have been able to evaluate the effects of including fault tolerance in an embedded system.

This paper is organized as follows. Section 2 describes the embedded system used, as well as the ECCs added. Section 3 reports the results of the evaluation of the fault-tolerant embedded system. Finally, Section 4 concludes this work.

2 System description

2.1 Characteristics of the embedded system

To implement our embedded system, we have utilized the STM32F429i-DISC0VERY card [16]. It incorporates a development kit with an ARM Cortex-M4 architecture. Other characteristics of this card are [16]:

- 2.4'' QVGA TFT LCD.
- External 64 Mbit SDRAM.
- Integrated debugging tool.
- A set of sensors and actuators (LEDs, gyroscope, and some buttons).

We have also included an RGB LED and a temperature and humidity sensor. The RGB LED will turn on different colors depending on the value of temperature and humidity obtained from the sensor.

We have implemented a simple control system that will allow us to study the effects of the inclusion of ECCs. Data provided by the humidity and temperature sensor will be protected by using different ECCs, as the behavior of the system depends on this data. Fig. 1 shows the system flow diagram.

Once obtained the values of temperature and humidity, they are protected by applying different ECCs (that will be explained next). In addition, values of humidity and temperature are shown on the LCD screen, and the RGB LED will be activated too. The idea is to protect and verify that the data obtained from the humidity and temperature sensor is correct, without delaying new measurements.

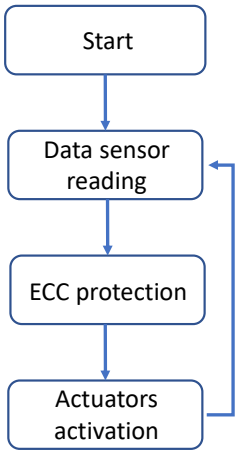

Fig. 1. Flow diagram of the control algorithm [13].

2.2 Error Correction Codes used

We have used two families of ECCs in our study [13], [14], [15], [17], [20]. They present different encoding and decoding functions with diverse error coverages. In this way, we can study the influence of these ECCs in the execution time and the software size. We must comment that we have used software versions of these ECCs, although they were designed to be implemented in hardware.

Ultrafast Codes

Introduced in [17], Ultrafast ECCs were designed with the main purpose of reducing encoding and decoding latencies. These ECCs present a high redundancy, compensated by a really good processing speed. In this way, Ultrafast ECCs are especially suitable for systems in which processing speed is essential. In the present work, only two variables are being protected, so the redundancy of the ECCs used is acceptable.

The parity check matrix **H** that defines the ECC (extracted from [17]) is shown in Fig. 2. As it can be seen, it is formed by an identity matrix (I_{8x8}) for the parity bits part. Data bits part are represented by A_{8x8}. Specifically, this matrix defines an ECC that can correct single errors (SEC – *Single Error Correction*), up to 5 adjacent errors (5AEC – 5 *Adjacent Error Correction*), and detect 2 non-adjacent errors (DED – *Double Error Detection*). This ECC is denoted as (16, 8) SEC-5AEC-DED.

It is possible to design various decoders with different error coverages from the parity check matrix shown in Fig. 2. Even, we can combine diverse encoders and decoders for the protection of longer data words. In addition, ECCs for data words of 16, 32, and 64 bits (or longer lengths) can be generated. As examples, Fig. 3 and Fig. 4 present parity check matrices for 16- and 32-bit data words, respectively.

We can get **H16** by interleaving two **H8** matrices. This new **H16** matrix represents an Ultrafast (32, 16) SEC-10AEC-DED, where $c_{i\ \mathbf{H8}}$ represents the *i*-th column of the

H8 matrix. As it can be observed, a 10-bit adjacent error is treated as two 5-bit adjacent errors, which can be corrected by each original code.

This matrix (shown in Fig. 3) can be generalized for other word lengths (32, 64, … bits), as shown in Fig. 4 for the case of data words of 32 bits.

$$H_8 = [\mathbf{I}_{8\times8} \quad \mathbf{A}_{8\times8}] = \begin{bmatrix} 10000000 & 10100010 \\ 01000000 & 01000101 \\ 00100000 & 10101000 \\ 00010000 & 01010100 \\ 00001000 & 10001010 \\ 00000100 & 01010001 \\ 00000010 & 00101010 \\ 00000001 & 00010101 \end{bmatrix}$$

Fig. 2. Parity check matrix **H** with 8 bits of data and 8 redundant bits [17].

$$\mathbf{H16} = \begin{bmatrix} c_0\,\mathbf{H8} & \mathbf{0}_{8\times1} & c_1\,\mathbf{H8} & \mathbf{0}_{8\times1} & \dots \\ \mathbf{0}_{8\times1} & c_0\,\mathbf{H8} & \mathbf{0}_{8\times1} & c_1\,\mathbf{H8} & \end{bmatrix}$$

Fig. 3. Parity check matrix **H** with 16 bits of data and 16 redundant bits [17].

$$\mathbf{H32} = \begin{bmatrix} c_0\,\mathbf{H8} & \mathbf{0}_{8\times1} & \mathbf{0}_{8\times1} & \mathbf{0}_{8\times1} & c_1\,\mathbf{H8} & \\ \mathbf{0}_{8\times1} & c_0\,\mathbf{H8} & \mathbf{0}_{8\times1} & \mathbf{0}_{8\times1} & \mathbf{0}_{8\times1} & \dots \\ \mathbf{0}_{8\times1} & \mathbf{0}_{8\times1} & c_0\,\mathbf{H8} & \mathbf{0}_{8\times1} & \mathbf{0}_{8\times1} & \\ \mathbf{0}_{8\times1} & \mathbf{0}_{8\times1} & \mathbf{0}_{8\times1} & c_0\,\mathbf{H8} & \mathbf{0}_{8\times1} & \end{bmatrix}$$

Fig. 4. Parity check matrix **H** with 32 bits of data and 32 redundant bits [17].

In the present work, diverse ECCs for data words of 32 bits have been used. Their main difference is their capabilities to correct adjacent errors: i) SEC-DED-8AEC; ii) SEC-DED-12AEC; iii) SEC-DED-16AEC; and iv) SEC-DED-20AEC.

All these ECCs can correct up to 8-bit burst errors and detect up to 12-bit burst errors. In addition, each one of them can correct the adjacent errors pointed (8, 12, 16 and 20). This error coverage has been achieved by using interleaving [18], [19]. More information can be seen in [13], [17].

Matrix-based Low Redundant Code

The second ECC was presented in [20]. This ECC introduces only 8 parity bits to protect 32-bit data words. This lower number of code bits causes a lower coverage with respect to Ultrafast codes. The parity matrix **H** that defines the ECC can be seen in Fig. 5. This ECC is a Matrix-based ECC. It organizes data and parity bits according to Fig. 6.

This ECC can correct single errors, as well as 2- and 3-bit adjacent errors in rows (horizontal pattern) and columns (vertical pattern). In addition, this ECC can correct

errors in a 2x2 square pattern, that is, errors affecting 2 neighbour rows and 2 neighbour columns.

$$\mathbf{H} = \begin{array}{c} C_0 C_1 \cdots\cdots C_7 X_0 X_1 \cdots\cdots X_{31} \\ \left|\begin{array}{l} 10000000001010001000101001000001100101 01 \\ 01000000100001010101000010110100000100 10 \\ 00100000010100000000100100100101010010 10 \\ 00010000100000100000100101011000101001 01 \\ 00001000010001000010001010100111010001 00 \\ 00000100001100100100011100010000000010 11 \\ 00000010000010010010000011100101101010 00 \\ 00000001000000001001010100101010110101 00 \end{array}\right| \end{array}$$

Fig. 5. Parity check matrix **H** with 32 bits of data and 8 redundant bits [20].

C_0	C_1	C_2	C_3	C_4	C_5	C_6	C_7
X_0	X_1	X_2	X_3	X_4	X_5	X_6	X_7
X_8	X_9	X_{10}	X_{11}	X_{12}	X_{13}	X_{14}	X_{15}
X_{16}	X_{17}	X_{18}	X_{19}	X_{20}	X_{21}	X_{22}	X_{23}
X_{24}	X_{25}	X_{26}	X_{27}	X_{28}	X_{29}	X_{30}	X_{31}

Fig. 6. Layout of the second ECC [20].

3 Evaluation

Table I presents the software sizes of the implementation of the different ECCs. As expected, software size of Ultrafast ECCs grows with the error coverage. A higher error coverage is accomplished with formulas that are more complex during encoding and decoding processes. Biggest software size corresponds to the Matrix-based ECC. This increment is caused by two factors: i) the special layout of the code; and ii) the low number of redundant bits. These elements provoke more complex processes to encode and decode data, that is translated into a bigger software size.

Table 1. Size of software.

System	Size
Non-Protected System	21.0 KB
SEC-DED-8AEC	29.0 KB
SEC-DED-12AEC	33.4 KB
SEC-DED-16AEC	35.0 KB
SEC-DED-20AEC	40.6 KB
Matrix-based ECC	51.6 KB

We have also studied the execution time of the Ultrafast codes, as these ECCs present the biggest error coverages and the lowest software sizes. Table 2 shows the results obtained.

Table 2. Execution time of Ultrafast codes [13].

System	Encoder	Decoder	Total
SEC-DED-8AEC	71.1 ms	103.53 ms	175.3 ms
SEC-DED-12AEC	71.1 ms	118.03 ms	189.8 ms
SEC-DED-16AEC	71.1 ms	130.23 ms	202 ms
SEC-DED-20AEC	71.1 ms	161.93 ms	233.7 ms

As we can see, the encoder execution time is the same for all the ECCs. This is an expected result, as we have used the same encoder for all ECCs. With respect to the decoding time, it follows the same trend than software size: a bigger fault tolerance capacity carries on a bigger execution time.

The total execution time shown in Table 2 also includes the execution time of a fault injection routine used to check the correct operation of the system. This routine takes 0.67 ms.

Fault injection is an experimental validation technique of fault tolerant systems that consists in the intentional introduction of errors into the system in order to verify that the fault-tolerance mechanisms accomplish their design specifications [21], [22]. Specifically, in this work, we have used software fault injection. It can be applied at compilation time or at execution time:

- Software fault injection at compilation time modifies the source code to simulate faults.
- Software fault injection at execution time simulates the occurrence of a fault by modifying one (or several bits) in the memory (data or code) or in the CPU registers.

In this paper, we have used software fault injection at execution time. Thus, we have been able to check the correct behaviour of the ECCs. Fault injection has been carried out by instrumentalizing the code through a small fault injection routine. Fault model used has been *bit-flip*. Single *bit-flips* (affecting a single bit) and multiple *bit-flips* (affecting several bits) have been injected. Multiple faults can be adjacent (alteration of various contiguous bits) or burst (contiguous bits in which we are only sure that the first and last bits are erroneous).

Faults have been injected in the variables that store the values of temperature and humidity, as these are the critical variables of the system, and thus, they are protected by the ECCs. The rest of variables used are not protected since they are reset each time they are employed.

The results obtained show the viability of protecting data by using a software implementation of the ECCs. In this way, there are two factors to consider:

i. Time needed by the Embedded System to perform its control loop. In our case, the specifications of the temperature/humidity sensor indicate that measurements can be taken every two seconds. All our ECCs can perform all their functions within this period.

ii. Software size is small enough to be stored in the Embedded System memory.

4 Conclusions

In this work, we have seen that it is possible to use ECCs in Embedded Systems. We have protected, by means of various ECCs with different fault tolerance properties, a series of variables to check the viability of this protection. We have seen that the implementation of the ECCs is viable, even using ECCs with a great number of redundant bits, as we are protecting only a limited number of variables, instead of the complete memory.

We have been able to verify that the ECCs used are adequate in processes with low latencies. In addition, we have used interleaving to increase the fault tolerance of the original ECCs.

In the future, we want to carry out more tests, increasing the complexity of the embedded system, adding a greater number of sensors and actuators, expanding the number of variables to protect, using other types of microprocessors, such as Arduino, and checking other types of ECCs.

References

1. The International Technology Roadmap for Semiconductors 2013. [Online]. Available at: http://www.itrs2.net/2013-itrs.html
2. E. Ibe, H. Taniguchi, Y. Yahagi, K. Shimbo, and T. Toba, "Impact of scaling on neutron-induced soft error in SRAMs from a 250 nm to a 22 nm design rule", IEEE Trans. Electron Devices, vol. 57, no. 7, pp. 1527–1538, July 2010.
3. G. Tsiligiannis et. al., "Multiple Cell Upset Classification in Commercial SRAMs", IEEE Transactions on Nuclear Science, vol. 61, no. 4, August 2014.
4. N.G. Chechenin and M. Sajid, "Multiple cell upsets rate estimation for 65 nm SRAM bit-cell in space radiation environment", 3rd International Conference and Exhibition on Satellite & Space Missions, May 2017.
5. E. Fujiwara, Code Design for Dependable Systems: Theory and Practical Application, Ed. Wiley-Interscience, 2006.
6. R. W. Hamming, "Error detecting and error correcting codes," Bell System Technical Journal, vol. 29, pp. 147–160, 1950.
7. C.L. Chen and M.Y. Hsiao, "Error-correcting codes for semiconductor memory applications: a state-of-the-art review", IBM Journal of Research and Development, vol. 58, no. 2, pp. 124–134, March 1984.
8. J. Gracia-Moran, L.J. Saiz-Adalid, D. Gil-Tomás, and P.J. Gil-Vicente, "Improving Error Correction Codes for Multiple Cell Upsets in Space Applications", IEEE Transactions on Very Large Scale Integration (VLSI) Systems, vol. 26(10), pp. 2132-2142, October 2018.
9. H.S. de Castro, et al. "A correction code for multiple cells upsets in memory devices for space applications", 2016 14th IEEE International New Circuits and Systems Conference (NEWCAS 2016), pp.1–4, June 2016.
10. A. Sánchez-Macián, P. Reviriego, J. Tabero, A. Regadío and J.A. Maestro, "SEFI protection for Nanosat 16-bit Chip On-Board Computer Memories", IEEE Transactions on Device and Materials Reliability, vol. 17(4), pp. 698-707, December 2017.
11. C. Argyrides, D.K. Pradhan, and T. Kocak, "Matrix codes for reliable and cost efficient memory chips", IEEE Transactions on Very Large Scale Integration (VLSI) Systems, vol. 19, nº 3, pp.420–428, March 2011.
12. https://www.maximintegrated.com/en/products/microcontrollers/MAX32670.html

13. J. Gracia-Morán, P. Martín-Tabares, L.J. Saiz-Adalid, “Estudio del impacto de la inclusión de Códigos Correctores de Errores en un Sistema Empotrado”, V Jornadas de Computación Empotrada y Reconfigurable (JCER2020/2021), Jornadas SARTECO, pp. 647-651, ISBN: 978-840932487-3, September 2021.
14. C. Martínez-Ruiz, “Desarrollo e implementación de un sistema empotrado con propiedades de tolerancia a fallos para sistemas de confort de vehículos autónomos”, Final Degree Project, Escuela Técnica Superior de Ingeniería Industrial, Universitat Politècnica de València, http://hdl.handle.net/10251/160339, February 2021
15. P. Martín-Tabares, “Desarrollo e implementación de un sistema empotrado tolerante a fallos para el control de condiciones meteorológicas”, Final Degree Project, Escuela Técnica Superior de Ingeniería Industrial, Universitat Politècnica de València, https://riunet.upv.es/handle/10251/165336, March 2021.
16. ST-Elcctronics. "User Manual. Discovery kit with STM32F429ZI MCU". https://www.st.com/resource/en/user_manual/dm00093903-discovery-kit-with-stm32f429zi-mcu-stmicroelectronics.pdf
17. L.J. Saiz-Adalid, J. Gracia-Morán, D. Gil-Tomás, J.C. Baraza-Calvo and P.J. Gil-Vicente, “Ultrafast Codes for Multiple Adjacent Error Correction and Double Error Detection,” IEEE Access, vol. 7, pp. 151131-151143, 2019, doi: 10.1109/ACCESS.2019.2947315.
18. L.J. Saiz-Adalid, P. Gil-Vicente, J. Gracia-Morán, and J.C. Baraza-Calvo, “Using Interleaving to Avoid the Effects of Multiple Adjacent Faults in On-Chip Interconnection Lines”, 14th European Workshop on Dependable Computing (EWDC 2013), pp. 198-201, May 2013.
19. S. Baeg, S. Wen, R. Wong, “SRAM interleaving distance selection with a soft error failure model”, IEEE Transactions on Nuclear Science, 56 (4), pp. 2111-2118, Agosto 2009.
20. J. Gracia-Morán, L.J. Saiz-Adalid, J.C. Baraza-Calvo, P.J. Gil-Vicente, “Correction of Adjacent Errors with Low Redundant Matrix Error Correction Codes”, 8th Latin-American Symposium on Dependable Computing (LADC 2018), pp. 107-114, October 2018.
21. A. Benso and P. Prinetto, “Fault Injection Techniques and Tools for Embedded Systems”, Springer, 2003.
22. D. Gil-Tomás, J. Gracia-Morán, J.C. Baraza-Calvo, L.J. Saiz-Adalid and P. Gil-Vicente, “Injecting Intermittent Faults for the Dependability Assessment of a Fault-Tolerant Microcomputer System”, IEEE Transactions on Reliability, vol. 65, no. 2, pp. 648-661, June 2016, doi: 10.1109/TR.2015.2484058.

Tolerating Double and Triple Random Errors with Low Redundancy Error Correction Codes[1]

J. Gracia-Morán*, L.J. Saiz-Adalid*, J.C. Baraza-Calvo*,
D. Gil-Tomás*, P.J. Gil-Vicente*

* Instituto ITACA, Universitat Politècncia de València
Camino de Vera, s/n, 46022 Valencia, Spain
{jgracia, ljsaiz, jcbaraza, dgil, pgil}@itaca.upv.es

Abstract. With the continuous size reduction of CMOS technology, faults suffered by RAM memory systems are more likely. Thus, the probability of occurrence of Multiple Cell Upsets (MCUs), in addition to Single Cell Upsets (SCUs), augments. Traditionally, Error Correction Codes (ECCs) are a family of Fault Tolerance Mechanisms (FTMs) that have been used to protect memories. An aspect to consider when designing ECCs is the area, delay, and power consumption overheads that encoder and decoder circuits introduce, as well as the number of redundant bits used by the Error Correction Code.
In this work, we introduce a series of new low redundancy Error Correction Codes specially designed to correct multiple random errors. We have compared error coverage and overheads introduced by these new codes with other well-known ones. In this way, we have been able to study the influence of this low redundancy in the area, power consumption, and delay overheads.

1 Introduction

As CMOS technology continues its physical downscaling, the fault rate of these circuits also augments [1]. For instance, thanks to this scale reduction, memory systems can provide a great storage capacity. Nevertheless, this reduction causes an increment in their fault rate, due to the decrease of the memory cell critical charge and the energy needed to cause a Single Event Upset (SEU). In fact, Multiple Cell Upsets (MCUs) can also be induced by a single particle hit [2][4][5]. When a memory cell is impacted by a cosmic particle, a flow of electron-hole pairs occurs along the transport track [7]. In this way, multiple random errors, as well as adjacent errors, can be generated. In the case of critical applications, the MCU problem must be considered when designing fault tolerance methods [3][6].

Broadly used methods to protect memory systems are Error Correction Codes (ECCs). Common ECCs used to protect standard memories are Single Error Correction (SEC) codes or Single Error Correction-Double Error Detection (SEC-DED) codes [8] [9][10]. In critical applications, more complex and sophisticated codes are used [11] [12][13][14][15].

[1] Grant PID2020-120271RB-I00 funded by MCIN/AEI/10.13039/501100011033.

C.Fernandez-Llatas and M.Guillen (Ed.):
Workshop on Innovation on
Information and Communication Technologies
(ITACA-WIICT 2022)

ISBN 978-84-09-46075-5

The introduction of an ECC in memory implies the addition of several redundant bits, also called code bits or parity bits. These extra bits, that are used to detect and/or correct the possible errors produced, must be also stored in memory. In this way, the number of code bits should be as low as possible, as they are added to each word of the memory. For example, a 2GB memory with an ECC with 100% of redundancy means that only 1GB is available to store the payload (the "raw" data). The remaining 1GB is required for the code bits. Different works have presented ECCs with low redundancy, such as [16][17][18][19]. All these works focus on adjacent errors. In the case of low redundancy ECCs designed to tolerate multiple random errors, binary BCH codes have been traditionally proposed [20][21][22]. These cyclic codes are a generalization of Hamming codes for multiple error correction.

On the other hand, another aspect to consider are the overheads in the area, power consumption and delay that encoders and decoders add. Also, these overheads should be maintained as low as possible. For instance, when redundancy is not the main issue, different approaches to reduce area, power consumption and delay can be used. Matrix codes [12][13] are a well-known type of ECC that uses a two-dimensional scheme. By combining two, or more, simpler error detection and/or correction methods, they achieve greater reliability.

In this paper, we present some new ECCs whose main characteristic is their low redundancy. They all have been developed by using a methodology elaborated by the authors [24]. This design methodology has been proven to be very useful to design efficient ECCs that can tolerate MCUs [14][15][22][23]. Specifically, the ECCs introduced in this work can correct 2- or 3-bit random errors. To evaluate these new proposals, fault injection and synthesis in 45 nm technology have been used.

This work is organized as follows. Section 2 presents some traditional ECCs, used as a basis to other ECCs or proposed for critical applications. Section 3 introduces our proposals. Section 4 describes the different results obtained during the evaluation of the ECCs. Finally, Section 5 concludes this paper.

2 Traditional Error Correction Codes

2.1 Hamming codes

Developed by Richard W. Hamming [9], Hamming codes were one of the first ECCs used to get data reliability. Hamming SEC (Single Error Correction) codes can correct 1-bit errors with the lowest redundancy. A given linear block code can be described by its parity check matrix **H**. For example, the matrix for the Hamming (7, 4) ECC is shown in (1), being $n = 7$ the number of bits of the codeword, and $k = 4$ the number of bits of the data word. Using this parity check matrix, the encoding formulas can be obtained as shown in Table 1.

It is possible to determine the syndrome bits in the same way, as shown in Table 2. The received word is correct when all syndrome bits are equal to zero. Otherwise, the word is erroneous, and syndrome bits are used to locate the erroneous bit using a lookup

table. Focusing on common word lengths (8, 16, 32 and 64), there exist (12, 8), (21, 16), (38, 32) and (71, 64) SEC Hamming codes respectively.

$$\mathbf{H} = \begin{bmatrix} 1010101 \\ 0110011 \\ 0001111 \end{bmatrix} \quad (1)$$

Table 1. Encoding formulas for Hamming SEC (7, 4)

b_0	b_1	b_2	b_3	b_4	b_5	b_6	*Encoding formulas*
		u_0		u_1	u_2	u_3	
1	0	1	0	1	0	1	$b_0 = u_0 \oplus u_1 \oplus u_3$
0	1	1	0	0	1	1	$b_1 = u_0 \oplus u_2 \oplus u_3$
0	0	0	1	1	1	1	$b_3 = u_1 \oplus u_2 \oplus u_3$

Table 2. Syndrome calculation for Hamming SEC (7, 4)

r_0	r_1	r_2	r_3	r_4	r_5	r_6	*Syndrome bits*
		u_0		u_1	u_2	u_3	
1	0	1	0	1	0	1	$s_0 = r_0 \oplus r_2 \oplus r_4 \oplus r_6$
0	1	1	0	0	1	1	$s_1 = r_1 \oplus r_2 \oplus r_5 \oplus r_6$
0	0	0	1	1	1	1	$s_2 = r_3 \oplus r_4 \oplus r_5 \oplus r_6$

By including an additional parity bit, it is possible to achieve double error detection. That is, with this extra bit it is possible to implement Extended Hamming codes that are SEC-DED (Single Error Correction – Double Error Detection). This extra bit calculates the even parity of the whole encoded word. In this way, there exist (13, 8), (22, 16), (39, 32) and (72, 64) SEC-DED extended Hamming codes. An aspect to be considered is that the logic depth of the encoding and decoding circuits scales with the word length. Thus, the latency introduced by these circuits grows with longer words.

2.2 Hsiao codes

Hsiao codes are an optimized version of extended Hamming codes [25]. The parity check matrix of a Hsiao code must fulfil these requirements:

- Each column must be different and nonzero.
- Every column contains an odd number of 1s.
- The total number of 1s in the parity check matrix should be minimum.
- The number of 1s in each row should be made equal, or as close as possible, to the average number.

As an example, Table 3 and Table 4 show the parity check matrix and the syndrome calculation, respectively, for an (8, 4) Hsiao code.

Table 3. Encoding formulas for Hsiao SEC-DED (8, 4)

b_0	b_1	b_2	b_3	b_4	b_5	b_6	b_7	***Encoding formulas***
				u_0	u_1	u_2	u_3	
1	0	0	0	0	1	1	1	$b_0 = u_1 \oplus u_2 \oplus u_3$
0	1	0	0	1	0	1	1	$b_1 = u_0 \oplus u_2 \oplus u_3$
0	0	1	0	1	1	0	1	$b_2 = u_0 \oplus u_1 \oplus u_3$
0	0	0	1	1	1	1	0	$b_3 = u_0 \oplus u_1 \oplus u_2$

Table 4. Syndrome calculation for Hsiao SEC-DED (8, 4)

r_0	r_1	r_2	r_3	r_4	r_5	r_6	r_7	***Syndrome bits***
				u_0	u_1	u_2	u_3	
1	0	0	0	0	1	1	1	$s_0 = r_0 \oplus r_5 \oplus r_6 \oplus r_7$
0	1	0	0	1	0	1	1	$s_1 = r_1 \oplus r_4 \oplus r_6 \oplus r_7$
0	0	1	0	1	1	0	1	$s_2 = r_2 \oplus r_4 \oplus r_5 \oplus r_7$
0	0	0	1	1	1	1	0	$s_3 = r_3 \oplus r_4 \oplus r_5 \oplus r_6$

The decoding process is equal to the Hamming codes' one explained before. All syndrome bits are zero when no error occurs. If a single error occurs, syndrome presents an odd number of 1s, and it is equal to the column corresponding to the erroneous bit. When a 2-bit error occurs, a nonzero syndrome with an even number of 1s is obtained. In any case, a binary decoder taking the syndrome as input can handle both the selection of the erroneous bit and the activation of a NRE (*non-recoverable error*) condition.

2.3 BCH codes

Binary BCH codes are a generalization of Hamming codes for multiple error correction. They form a large class of random error-correcting cyclic codes with a low number of redundancy bits [20][21].

Specifically, to define a binary BCH code, for any positive integer $m \geq 3$ and $t \geq 2^{m-1}$ (error-correcting capability), there exists a binary *t*-error-correcting BCH code, denoted as BCH (*n*, *k*, *d*), with the following parameters:

- Codeword length: $n = 2^m - 1$
- Number of redundancy bits: $n - k = mt$
- Minimum Hamming distance: $d_{min} \geq 2t + 1$

where *n* is the size of the codeword, *k* is the length of the data word, d_{min} is the minimum Hamming distance, and *t* is the number of correctable errors.

To form the codewords, the remainder of a polynomial representing our information bits divided by a generator polynomial is taken. This generator polynomial is selected to give the code its characteristics. In this way, all codewords are multiples of the generator polynomial.

2.4 Matrix-based Error Correction Codes

Matrix-based ECCs combine two or more types of Error Correction methods to detect and/or correct different types of errors [12][13]. Matrix-based codes form a two-dimensional scheme, in such a way that combining several correction methods the general error correction coverage is increased. Usually, diverse types of Hamming codes are combined with parity checks.

An example of matrix code is the ECC introduced in [12], whose layout can be seen in Fig. 1. In this figure, X_i are the data bits, C_j are the horizontal check bits (calculated using a pseudo SEC-DED Hamming code), and P_k are the column parity bits (calculated using even parity). By combining Hamming codes and parity checks, this ECC (hereafter we will refer to it as Matrix code) forms a two-dimensional scheme for correcting some patterns of MCUs [12] by using a total of 28 code bits.

X_0	X_1	X_2	X_3	X_4	X_5	X_6	X_7	C_0	C_1	C_2	C_3	C_4
X_8	X_9	X_{10}	X_{11}	X_{12}	X_{13}	X_{14}	X_{15}	C_5	C_6	C_7	C_8	C_9
X_{16}	X_{17}	X_{18}	X_{19}	X_{20}	X_{21}	X_{22}	X_{23}	C_{10}	C_{11}	C_{12}	C_{13}	C_{14}
X_{24}	X_{25}	X_{26}	X_{27}	X_{28}	X_{29}	X_{30}	X_{31}	C_{15}	C_{16}	C_{17}	C_{18}	C_{19}
P_0	P_1	P_2	P_3	P_4	P_5	P_6	P_7					

Fig. 1. Matrix-based ECC from [12]

3 Our Proposals: Low Redundancy (LR) ECCs

In this section, we introduce some new low redundancy ECCs able to correct MBUs. They have been generated by using a methodology developed by the authors [24]. Their main objective is to reduce the number of redundant bits, while maintaining (or even increasing) the error coverage with respect to other well-known codes. All codes presented have been applied to 32-bit data words.

The first proposal, named LR DEC (48, 32), can correct single and 2-bit random errors with only 16 redundant bits. The parity matrix **H** of this code can be seen in Fig. 2, where X_j are the data bits and C_i are the code bits.

Our second proposal, called LR TEC (50, 32), can correct up to 3-bit random errors with only 2 more redundant bits than the LR DEC (48, 32). The parity matrix **H** of this code can be seen in Fig. 3.

The last proposal adds other 2 extra bits to get an ECC that can correct up to 3-bit random errors. The parity check matrix **H** of this code is presented in Fig. 4. The objective of this code is to reduce the area, power consumption and delay overheads with respect to the LR TEC (50 32) ECC by simplifying the encoding and decoding circuitry.

$$H = \begin{array}{c} \begin{matrix} C_0 C_1 \cdots\cdots\cdots\cdots\cdots C_{15} X_0 \cdots\cdots\cdots\cdots\cdots\cdots\cdots\cdots\cdots\cdots\cdots\cdots\cdots\cdots X_{31} \end{matrix} \\ \begin{bmatrix} 10000000000000000111100110111000000000000000000000 \\ 01000000000000000111001110010001101000000000000000 \\ 00100000000000000110111100000101100001000000000000 \\ 00010000000000000101010101001000101001001000000000 \\ 00001000000000000100101010111001001000001000000000 \\ 00000100000000000110101001101000010000010100000000 \\ 00000010000000000101010100010100100001100000100000 \\ 00000001000000000011000110011001001001000010000000 \\ 00000000100000000000110011000100101000100100010000 \\ 00000000010000000000011110000001001000011001010000 \\ 00000000001000000000000011110000100100000110110000 \\ 00000000000100000000000000011100010001111010010000 \\ 00000000000010000000000000001001001111100101010000 \\ 00000000000001000000000000000100111110001110011000 \\ 00000000000000100000000000000011111110000001111000 \\ 00000000000000010000000000000000000001111111111000 \end{bmatrix} \end{array}$$

Fig. 2. Parity matrix **H** of LR DEC (48, 32)

$$\mathbf{H} = \begin{array}{c} \begin{matrix} C_0 C_1 \cdots\cdots\cdots\cdots\cdots C_{15} X_0 \cdots\cdots\cdots\cdots\cdots\cdots\cdots\cdots\cdots\cdots\cdots\cdots\cdots\cdots X_{31} \end{matrix} \\ \begin{bmatrix} 10000000000000000011100010011010100000110101100000 \\ 01000000000000000011010001110110011101000000000010 \\ 00100000000000000011001100101001101100000010100001 \\ 00010000000000000010110101001011101010100000000100 \\ 00001000000000000010101011100101000000000001010010 \\ 00000100000000000010011110010100000001110010011000 \\ 00000010000000000011101101001110001000100000000001 \\ 00000001000000000011011010101000010010010001001010 \\ 00000000100000000001011011001000010010100001000001 \\ 00000000010000000000111000111000000010010101010011 \\ 00000000001000000000000111111000000000000110010110 \\ 00000000000100000000000000010011011000110001100111 \\ 00000000000010000000000000001101100010101100101100 \\ 00000000000001000000000000000101101010110001000000 \\ 00000000000000100000000000000011100110000100100111 \\ 00000000000000010000000000000000011110001100011010 \\ 00000000000000001000000000000000000011111000011100 \\ 00000000000000000100000000000000000000001111111100 \end{bmatrix} \end{array}$$

Fig. 3. Parity matrix **H** of LR TEC (50, 32)

$$\mathbf{H} = \begin{array}{c} C_0 C_1 \cdots\cdots\cdots\cdots\cdots\cdots C_{15} X_0 \cdots\cdots\cdots\cdots\cdots\cdots\cdots\cdots\cdots\cdots X_{31} \\ \left[\begin{array}{l}
1000000000000000000011100010010011100000000000000000 \\
0100000000000000000011010001111010001000000000000000 \\
0010000000000000000011001100100101101000000000000000 \\
0001000000000000000010110101000110101000000000001000 \\
0000100000000000000010101011101100000000000000101000 \\
0000010000000000000010011110011001000000001001000000 \\
0000001000000000000001110110101110000000000000000100 \\
0000000100000000000001101101011001000000001000001000 \\
0000000010000000000001011011000100100011000000000000 \\
0000000001000000000000111000110000001000110100100000 \\
0000000000100000000000011111000001000010100101000000 \\
0000000000010000000000000000011000100101101010101010 \\
0000000000001000000000000000000110101010101010100100 \\
0000000000000100000000000000000100001111010110001100 \\
0000000000000010000000000000000011111011000100100001 \\
0000000000000001000000000000000001100110110110010010 \\
0000000000000000100000000000000000111011010110010001 \\
0000000000000000010000000000000001111000110010001100 \\
0000000000000000001000000000000000011111000111110011 \\
0000000000000000000100000000000000000000011111111111
\end{array}\right] \end{array}$$

Fig. 4. Parity matrix **H** of LR TEC (52, 32)

4 Evaluation of the Proposed Codes

In this section, we have compared the error coverage of different ECCs, as well as the overheads introduced by their encoders and decoders. This evaluation has been divided in two phases. First, we have injected faults in C models of the ECCs to measure the error coverage. Next, we have modelled the different ECCs in VHDL, and we have synthesized them to estimate area, power, and delay overheads. We have compared our proposals with different ECCs that implement diverse strategies to tolerate multiple faults in 32-bits data words. The codes used for comparison has been a Hsiao code [25], a BCH code [20], and a Matrix code [12], such as the ones presented previously.

4.1 Error coverage

Typically, errors can be classified in *single* (only one bit affected), or *multiple* (more than one bit are affected). *Single errors* are commonly produced by Single Event Upsets (SEU, in random access memories) or Single Event Transients (SET, in combinational logic) [27]. On the other hand, *multiple errors* are becoming more frequent. Due to the continuous increasing of the integration scale, the memory cell critical charge and the energy needed to provoke a SEU in storage have been reduced [3]. In addition, this

energy reduction can also provoke multiple-cell upsets (MCUs), that is, simultaneous errors in more than one memory cell induced by a single particle hit [3][4].

To evaluate the error coverage of the ECCs presented in previous sections, we have used a fault injection tool developed by the authors [14]. It allows injecting *single errors*, as well as *multiple errors* with different patterns and lengths.

To assess the error correction capabilities of the different ECCs, we have injected each type of error in each bit of the codeword. That is, we have not injected errors according to their probability of occurrence, as our objective has been to measure error correction coverages.

Thus, we have injected *single errors* in all bits of the codeword. Then, we have injected *double random errors* in all pairs of bits of the codeword, and so on up to eight random errors. Evidently, *multiple errors* of length 8 will be much less frequent than double errors [5][6], but this is not in the scope of this paper. The reason to inject up to 8 multiple random errors is that these ranges include typical values of MCUs in critical environments [4]. By injecting all errors of a given size and model (i.e. *random* or *adjacent*), we can count the number of corrected and/or detected errors with respect to the total number of possible errors, calculating the error coverage of each ECC.

For the calculus of the correction coverage, we have used formula (2), where $Errors\_Corrected$ is the number of errors corrected by the ECC, and $Errors\_Injected$ is the number of errors injected. For the detection coverage, we have used formula (3), where $Errors\_Detected$ corresponds to the number of errors detected but not corrected by the ECC.

$$C_{correc} = \frac{Errors\_Corrected}{Errors\_Injected} \times 100 \quad (\mathbf{2})$$

$$C_{detec} = \frac{Errors\_Corrected + Errors\_Detected}{Errors\_Injected} \times 100 \quad (\mathbf{3})$$

Fig. 5 shows the error correction coverage of all ECCs. As it can be seen, Hsiao and Matrix codes can only correct 1-bit errors. In the case of the Hsiao code, this is an expected result, as Hsiao code is SEC-DED (Single Error Correction-Double Error Detection). With respect to the Matrix code, it uses a Hamming code that can correct 2-bit errors only in the data bits (X_i bits, see Fig. 1). So, when an error affects both a data bit and a code bit (C_i bits) in the same row, it cannot be tolerated. For this reason, the percentage of 2-bit error correction is not 100%.

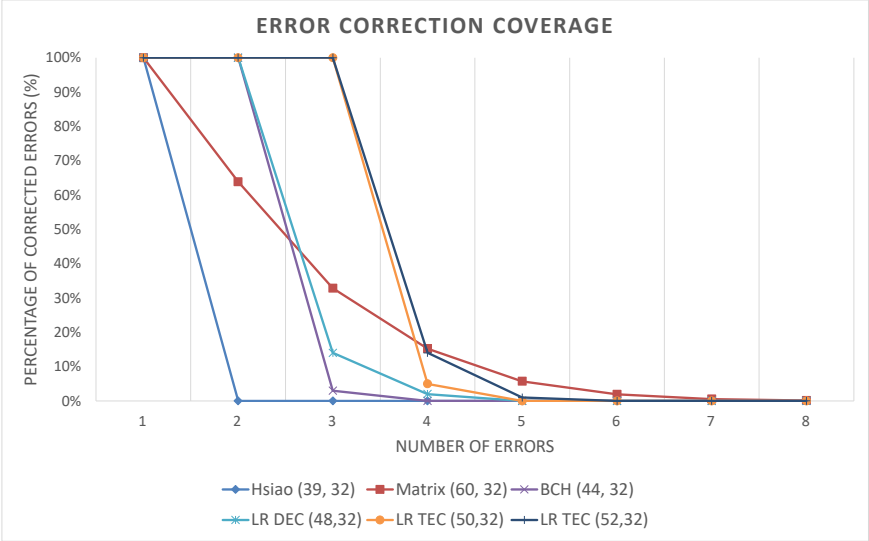

Fig. 5. Error correction coverage.

In the case of LR DEC (48, 32) and BCH (44,32), both codes can correct 2-bit errors. This is an expected result, as these codes have been designed with this requisite. Finally, LR TEC (50, 32) and LR TEC (52, 32) codes can correct up to 3 bits in error.

For longer error lengths, correction coverage decreases sharply. This result is provoked by the low number of redundant bits of the ECCs, that provoke a lower number of available syndromes to correct this type of errors.

On the other hand, Fig. 6 presents the error detection coverage. As it can be seen, Matrix code only ensures 100% of detection of single errors. As explained before, its DED capability only meets for errors in the data bits. Hsiao, BCH and LR DEC (48, 32) codes can detect all 2-bit random errors, and LR TEC (50, 32) and LR TEC (52, 32) codes can detect up to 3-bit random errors.

Regarding Hsiao code, we can see that in addition to 2-bit errors, it also detects almost 100% of the even-length errors. This behaviour is provoked by the DED capability of this code (it detects an even number of erroneous bits). For the rest of ECCs, detection coverage decreases for longer errors.

In summary, two of our proposals (LR TEC (50, 32) and LR TEC (52, 32)) present a higher error coverage, as they can correct up to 3-bit random errors. In the case of BCH and the LR DEC (48, 32) codes, they can correct up to 2-bit random errors, while Matrix and Hsiao codes can only correct 1-bit errors. An abstract of the different properties of the ECCs is shown in Table 5.

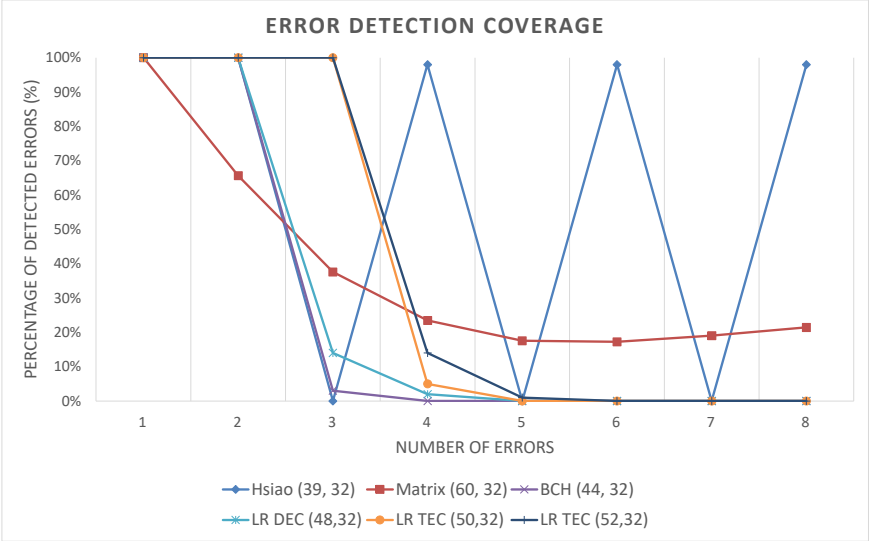

Fig. 6. Error detection coverage.

Table 5. Properties of the ECCs

ECC	Data bits *(k)*	Check bits *(n – k)*	Redundancy *(n – k)/k* (%)	Fault tolerance
Hsiao (39,32) [27]	32	7	21.9	Correction of single errors Detection of 2-bit errors
Matrix (60, 32) [15]	32	28	87.5	Correction of single errors Correction of 2-bit errors *in data*
BCH (44, 32) [24]	32	12	37.5	Correction of single errors Correction of 2-bit errors
LR DEC (48, 32)	32	16	50.0	Correction of single errors Correction of 2-bit errors
LR TEC (50, 32)	32	18	56.3	Correction of single errors Correction of 2-bit errors Correction of 3-bit errors
LR TEC (52, 32)	32	20	62.5	Correction of single errors Correction of 2-bit errors Correction of 3-bit errors

4.2 Synthesis results

Apart from improving the error coverage, the main characteristic of our proposals is their low redundancy for this error detection and correction capabilities, as shown in

Table 5. In this way, this lower redundancy provokes a lower storage requirement for the code bits.

Nevertheless, it is also interesting to study the complexity of the encoder and decoder circuitry of the different ECCs. In this section, and by using CADENCE software [28], we have carried out a logic synthesis for 45-nm technology by using the NanGate FreePDK45 Open Cell Library [29][30]. To do this, we have synthesized the encoder and decoder circuits for all ECCs by firstly implementing them in VHDL.

The idea is to study how this lower redundancy will affect the area, power consumption and delay overheads of the encoder and decoder circuits. Although the area overhead of these circuits may be negligible in comparison with memory overhead, power and delay overheads can be important, especially in critical systems. Results are shown in Tables 6, 7 and 8.

With respect to the area overhead, the greater fault tolerance properties of our proposals provoke higher area overheads. So that, Hsiao and Matrix codes present the lowest area overheads. As we have commented in previous section, these ECCs can correct only 1-bit errors. Regarding DEC codes (BCH and LR DEC (48, 32)), encoders show a similar area overhead, while the decoder area of BCH is bigger due to its lower number of redundant bits. Finally, the biggest decoder's area overhead corresponds to the two LR TEC codes (LR TEC (50, 32) and LR TEC (52, 32)). Their greater fault tolerance capabilities, together with the low number of redundant bits provoke such high overhead, mainly in the decoders. In the case of the encoders, though, they are slightly bigger than the DEC encoders.

Table 6. Area overheads of the ECCs (in μm^2)

ECC	Encoder	Decoder
Hsiao (39,32) [27]	214	413
Matrix (60, 32) [15]	251	766
BCH (44, 32) [24]	313	4658
LR DEC (48, 32)	330	3118
LR TEC (50, 32)	363	83734
LR TEC (52, 32)	373	56827

Regarding the delay overhead, the fastest encoder corresponds to Matrix. This is an expected result, as this ECC uses very simple formulas. The rest of encoders present a similar delay, except the BCH (44, 32) and the LR TEC (50, 32), that are somewhat bigger.

Table 7. Delay overheads of the ECCs (in ps)

ECC	Encoder	Decoder
Hsiao (39,32) [27]	328	413
Matrix (60, 32) [15]	251	486
BCH (44, 32) [24]	366	1388
LR DEC (48, 32)	302	1111
LR TEC (50, 32)	394	1832
LR TEC (52, 32)	310	2311

In the case of the decoders' delay, as Hsiao and Matrix codes present either lower error coverage or higher redundancy (or both), their delays are the lowest ones. Focusing on the DEC low redundancy codes (our LR DEC (48, 32) and the BCH), our proposal presents a lower delay. This score is provoked by its lower number of redundant bits. Finally, the highest decoder's delays correspond to the two TEC codes.

About power overhead, it is noticeable that lower area provokes lower power consumption. Hence, Hsiao and Matrix codes present the lowest power consumption overhead, mainly in the decoder's circuitry.

Table 8. Power consumption overheads of the ECCs (in mW)

ECC	Encoder	Decoder
Hsiao (39,32) [27]	0.202	0.426
Matrix (60, 32) [15]	0.220	0.609
BCH (44, 32) [24]	0.315	3.109
LR DEC (48, 32)	0.317	2.373
LR TEC (50, 32)	0.370	57.393
LR TEC (52, 32)	0.360	37.009

4.3 Estimated memory overhead

As commented before, our proposals need a low number of redundant bits to provide a good fault tolerance coverage. As these extra bits must be stored in memory, some memory overhead is produced. If we do not consider the contribution of encoders and decoders, we can approximate this overhead by knowing the memory area and power consumption, as well as the code redundancy.

We can define memory area and memory power overheads with formulas (4) and (5):

$$Mem\_Area_{overhead} = Mem\_Area \times Redundancy \quad (4)$$

$$Mem\_Power_{overhead} = Mem\_Power \times Redundancy \quad (5)$$

As a matter of example, we have synthesized a 64KB SRAM, which can be a typical configuration of a cache memory. Memory is organized in 16K words x 32 bits. The obtained values for the total area and power of the memory are:

$$Mem\_Area = 2972106\ \mu m^2 \approx 3\ mm^2$$

$$Mem\_Power = 137{,}4\ mW$$

Area and power overheads for this memory, estimated from equations (4) and (5), can be seen in Table 9. As shown, the lowest area and power overheads are obtained for the Hsiao code. Nevertheless, this ECC can only correct 1-bit errors. If bigger correction capabilities are needed, our proposals introduce lower overheads with higher fault tolerance properties. Furthermore, and according to the synthesis results, ECC encoder and decoder circuits are much smaller than memory array, thus the overhead of encoders and decoders can be offset by the reduction of the number of check bits in

each memory word. This reduction in hardware gives an additional benefit, as it tends to lower the chance of soft errors, increasing the reliability of the memory.

Table 9. Estimated memory overhead for a 64KB SRAM

ECC	Redundancy (%)	Estimated Area (mm^2)	Estimated Power (mW)
Hsiao (39,32) [27]	21.9	3.657	167.49
Matrix (60, 32) [15]	87.5	5.625	257.63
BCH (44, 32) [20]	37.5	4.125	188.93
LR DEC (48, 32)	50.0	4.500	206.10
LR TEC (50, 32)	56.3	4.689	214.76
LR TEC (52, 32)	62.5	4.875	223.28

5 Conclusions

In this work, we have proposed a group of new ECCs that are able to correct up to 2- or 3-bit random errors, and whose main characteristic is their low redundancy.

We have compared these proposals with other well-known ECCs, such as Hsiao, Matrix, and BCH codes. First, we have injected random single and multiple errors to evaluate the error correction and detection coverages of all ECCs. Then, we have synthesized the ECCs' encoders and decoders to measure their area, power consumption and delay overheads. Also, we have estimated area and power overheads if ECCs were added to an SRAM.

With respect to the error coverage, our proposals behave as expected: the LR DEC (48, 32) can correct single and 2-bit random errors, while the LR TEC (50, 32) and the LR TEC (52, 32) are able to correct single as well as 2- and 3-bit random errors.

ECCs with greater coverage causes greater area usage, power consumption and delay of the encoding and decoding processes. These overheads can be assumed when these ECCs are added to an SRAM.

In the future, we want to continue developing ECCs to decrease area, power, and delay overheads, while maintaining, or even increasing, the error coverage. Also, we want to study the impact of adding these ECCs to a microprocessor.

References

1. The International Technology Roadmap for Semiconductors 2013. [Online]. Available at: http://www.itrs2.net/2013-itrs.html
2. J. Barak, M. Murat, and A. Akkerman, "SEU due to electrons in silicon devices with nanometric sensitive volumes and small critical charge", Nuclear Instruments and Methods in Physics Research Section B: Beam Interactions with Materials and Atoms, vol. 287, pp. 113–119, September 2012.
3. E. Ibe, H. Taniguchi, Y. Yahagi, K. Shimbo, and T. Toba, "Impact of scaling on neutron-induced soft error in SRAMs from a 250 nm to a 22 nm design rule", IEEE Trans. Electron Devices, vol. 57, no. 7, pp. 1527–1538, July 2010.

4. G. Tsiligiannis et. al., “Multiple Cell Upset Classification in Commercial SRAMs”, IEEE Transactions on Nuclear Science, vol. 61, no. 4, pp. 1747-1754, August 2014.
5. G.I. Zebrev, “Multiple Cell Upset Cross-Section Uncertainty in Nanoscale Memories: Microdosimetric Approach”, 15th European Conference on Radiation and its Effects on Components and Systems (RADECS), September 2015.
6. N.G. Chechenin and M. Sajid, “Multiple cell upsets rate estimation for 65 nm SRAM bit-cell in space radiation environment”, 3rd International Conference and Exhibition on Satellite & Space Missions, May 2017.
7. N.N. Mahatme, B.L. Bhuva, Y.P. Fang, and A.S. Oates, “Impact of strained-Si PMOS transistors on SRAM soft error rates”, IEEE Transactions on Nuclear Science, vol. 59, no. 4, pp. 845–850, August 2012.
8. E. Fujiwara, Code Design for Dependable Systems: Theory and Practical Application, Ed. Wiley-Interscience, 2006.
9. R. W. Hamming, “Error detecting and error correcting codes,” Bell System Technical Journal, vol. 29, pp. 147–160, 1950.
10. C.L. Chen and M.Y. Hsiao, “Error-correcting codes for semiconductor memory applications: a state-of-the-art review”, IBM Journal of Research and Development, vol. 58, no. 2, pp. 124–134, March 1984.
11. A. Sánchez-Macián, P. Reviriego, J. Tabero, A. Regadío, and J.A. Maestro, “SEFI protection for Nanosat 16-bit Chip On-Board Computer Memories”, IEEE Transactions on Device and Materials Reliability, vo. 17(4), pp. 698-707, December 2017.
12. C. Argyrides, D.K. Pradhan, and T. Kocak, “Matrix codes for reliable and cost efficient memory chips”, IEEE Trans. on Very Large Scale Integration (VLSI) Systems, vol. 19, nº 3, pp.420–428, March 2011.
13. H.S. de Castro et al. “A correction code for multiple cells upsets in memory devices for space applications”, 2016 14th IEEE International New Circuits and Systems Conference (NEWCAS 2016), pp.1–4, June 2016.
14. J. Gracia-Morán, L.J. Saiz-Adalid, D. Gil-Tomás, P.J. Gil-Vicente, “Improving Error Correction Codes for Multiple-Cell Upsets in Space Applications”, IEEE Transactions on VLSI Systems, Vol. 26(10), pp. 2132-2142, October 2018.
15. J. Gracia-Moran, L.J. Saiz-Adalid, J.C. Baraza-Calvo, P.J. Gil-Vicente, “Correction of Adjacent Errors with Low Redundant Matrix Error Correction Codes”, 2018 Eighth Latin-American Symposium on Dependable Computing (LADC), pp. 107-114, October 2018.
16. L.J. Saiz-Adalid, P. Reviriego, P.J. Gil-Vicente, S. Pontarelli, and J.A. Maestro "MCU Tolerance in SRAMs Through Low-Redundancy Triple Adjacent Error Correction", IEEE Transactions on VLSI Systems, vol. 23, no. 10, pp. 2332-2336, October 2015.
17. Z. Ming, X.L. Yi, and L.H. Wei, "New SEC-DED-DAEC codes for multiple bit upsets mitigation in memory", 2011 IEEE/IFIP 19th International Conference on VLSI and System-on-Chip (VLSI-SoC), pp. 254-259, October 2011.
18. A.Dutta, "Low Cost Adjacent Double Error Correcting Code with Complete Elimination of Miscorrection within a Dispersion Window for Multiple Bit Upset Tolerant Memory", 2012 IEEE/IFIP 20th International Conference on VLSI and System-on-Chip (VLSI-SoC), October 2012.
19. A. Neale and M. Sachdev, "A New SEC-DED Error Correction Code Subclass for Adjacent MBU Tolerance in Embedded Memory", IEEE Transactions on Device and Materials Reliability, vol. 13(1), pp. 223-230, March 2013.
20. S. Lin and D.J. Costello, Error Control Coding, 2nd edition, Pearson-Prentice Hall, 2004.
21. R. Naseer and J. Draper, "DEC ECC design to improve memory reliability in Sub-100nm technologies", 2008 15th IEEE International Conference on Electronics, Circuits and Systems, pp. 586-589, August 2008.

22. L.J. Saiz-Adalid, J. Gracia-Morán, D. Gil-Tomás, J.C. Baraza-Calvo, P.J. Gil-Vicente, “Reducing the Overhead of BCH Codes: New Double Error Correction Codes”. Electronics. 2020; 9(11):1897. https://doi.org/10.3390/electronics9111897
23. L.J. Saiz-Adalid, J. Gracia-Morán, D. Gil-Tomás, J.C. Baraza-Calvo and P.J. Gil-Vicente, "Ultrafast Codes for Multiple Adjacent Error Correction and Double Error Detection," in IEEE Access, vol. 7, pp. 151131-151143, 2019, doi: 10.1109/ACCESS.2019.2947315.
24. L.J. Saiz-Adalid et al., "Flexible Unequal Error Control Codes with Selectable Error Detection and Correction Levels", 32th International Conference on Computer Safety, Reliability and Security (SAFECOMP 2013), pp. 178-189, September 2013.
25. M.Y. Hsiao, "A class of optimal minimum odd-weight column SEC-DED codes," IBM Journal of Research and Development, vol. 14, no. 4, pp. 395-401, July 1970.
26. P. Reviriego, S. Pontarelli, J. A. Maestro, and M. Ottavi, "A method to construct low delay single error correction (SEC) codes for protecting data bits only," IEEE Transactions on Computer-Aided Design of Integrated Circuits and Systems., vol. 32, no. 3, pp. 479-483, March 2013.
27. K.A. LaBel, "Proton single event effects (SEE) guideline", Submitted for publication on the NASA Electronic Parts and Packaging (NEPP) Program web site, August 2009. Available online: https://nepp.nasa.gov/files/18365/Proton_RHAGuide_NASAAug09.pdf
28. Cadence: EDA Tools and IP for System Design Enablement. Accessed: April 10, 2019. [Online]. Available: https://www.cadence.com
29. J. E. Stine et al., "FreePDK: An open-source variation-aware design kit," in Proc. IEEE Int. Conf. Microelectron. Syst. Educ. (MSE), pp. 173-174, June 2007.
30. NanGate FreePDK45 Open Cell Library. Accessed: April 10, 2019. [Online]. Available: https://www.eda.ncsu.edu/wiki/FreePDK45:Contents

Analysing the quality of inventors' country data at PATSTAT Global database

Jose-Mariano Dahoui-Obón[1,3], Carles Boronat-Moll[2], and Jose-Luis Hervas-Oliver[3]

[1] Institute of Information and Communication Technologies, Universitat Politècnica de València, Valencia, 46022, Spain
jodaob@itaca.upv.es
[2] Department of Business Administration, Universitat de València, Valencia, 46022, Spain
carles.boronat@uv.es
[3] Management Department, Universitat Politècnica de València, Valencia, 46022, Spain
jose.hervas@omp.upv.es

Abstract. Analyses of international collaboration based on patent indicators are conditioned by the availability of inventors' country data. This paper examines the availability of inventors' country information in the PATSTAT Global patent database over 13 decades and for several filing authorities. The large variability of the number of applications and available country data depending on the patent office and the range of years forces us to choose these parameters well to reduce the possibility of bias.

1 Introduction

Patents are industrial property titles granted by States, which recognise the right to exploit an invention exclusively for a limited time. In return, applicants must pay filing and maintenance fees and allow the invention to become part of state of the art through the publication of the patent application, favouring technological progress and more efficient use of research resources by avoiding investment in the development of what already exists.

The usefulness of patents does not end as a source of highly relevant technical information. The availability of patent data has facilitated the generation of different metrics and indicators that allow the assessment of the importance [1] and quality [2] of individual inventions and the business strategies [3] of the entities that generate them.

Patent databases are a valuable source of information for policymakers. They allow them to compare the performance of their nationals' inventions with those of other countries [4], detect international collaboration networks [5], and even analyse which organisations in other countries are benefiting from the inventiveness of their nationals [6]. Among these uses of patent indicators associated with the nationality of inventors is the assessment of the efficiency of programmes

C.Fernandez-Llatas and M.Guillen (Ed.):
Workshop on Innovation on
Information and Communication Technologies
(ITACA-WIICT 2022)

ISBN 978-84-09-46075-5

that finance the generation of innovations in collaboration with other countries. These programmes tend to promote international and interregional cooperation [7] as a way of structuring the territory at the level of knowledge generation and achieving excellence through combining the best talent, seeking to obtain high-value inventions that are more likely to reach the market and generate wealth.

When working with patent databases to calculate indicators associated with international collaboration, we find that country information is unavailable for some inventors and that some inventions even appear without declared inventors. There is a large variability in the percentage of patent applications with complete information on the inventors' nationality, depending on the patent office and the year. This makes us question whether this lack of information is entirely random or is introducing a bias since, for example, information on the origin of inventors is more likely to be available for those applications that belong to large patent families that are more valuable [8].

This paper aims to characterise a patent database to determine which national, international or regional authorities have the most accurate information on the inventors' country for which years. For this analysis, we have chosen PATSTAT Global 2020 Autumn Edition database. This work will make it possible to determine simply the patent offices and time intervals that offer the lowest risk of introducing biases in subsequent studies.

2 PATSTAT database

Designed to perform statistical analyses on patent data, the European Patent Office's PATSTAT Global database contains bibliographical information of more than 100 million patent documents from the mid-19th century up to today, covering the principal patent issuing authorities. PATSTAT can be provided as bulk data or consulted online. Looking for flexibility, we have chosen the offline version. A new version of PATSTAT is generated every six months (spring and autumn editions). In our case, we will work with the PATSTAT Global 2020 Autumn Edition. The most likely date for data extraction from the source databases is the end of July 2020.

2.1 Structure

PATSTAT Global consists of 29 tables with up to 38 fields. The main table is the patent application information table TLS201_APPLN and consists of 27 fields and more than 100 million records. The main field is the one that identifies the application "APPLN_ID" since it serves as a link with most of the other tables. In this table, we find several relevant fields to our study. Application Authority ("APPLN_AUTH") indicates the code of the patent office where the patent application has been filed. The field "APPLN_KIND" indicates the type of application. In our case, we will focus on types A (patents) and T (translations of granted PCT or EP applications). Following the usual practice of studies based

on patent data, we will use the priority year ("EARLIEST_FILING_YEAR") instead of the application year ("APPLN_FILING_YEAR") when classifying patents temporarily. Finally, the field that collects the number of inventors of an application ("NB_INVENTORS") will allow us to efficiently detect those applications that do not have information on the inventors.

PATSTAT does not treat applicants and inventors separately but considers them all within the person category, combining legal persons (e.g. enterprises) and physical persons. The table TLS207_PERS_APPLN, which links persons with applications, is particularly relevant. The field indicating the place in the list of inventors in the application ("NVT_SEQ_NR") allows separating persons who are not inventors with a value of 0.

The other significant table is the one that collects information on applicants and inventors (TLS206_PERSON). This table contains key data such as the country of residence ("PERSON_CTRY_CODE") (which is not necessarily the nationality).

Although we will not use it in our study, the table TLS226_PERSON_ORIG, which is a kind of unrefined version of the table TLS206_PERSON, may be of interest for some research. This table distinguishes between the country of the author and the country of the author's residence. Another table that we will not use is the one that links patent publications with persons (TLS227_PERS_PUBLN), and that can be used to analyse the changes of inventors at the times of their publication.

Finally, within the reference tables, TLS801_COUNTRY links country codes with information about states/countries/territories and IP organisations.

Further studies focusing on the calculation of patent indicators may require other tables. For example, to calculate the patent scope indicator, the table containing the international patent classification (IPC) codes linked to each application (TLS209_APPLN_IPC) and the table qualifying applications by technical field (TLS230_APPLN_TECHN_FIELD) are necessary.

3 Methodology

We will use the R programming language to process the database, as it has libraries especially prepared for the analysis and manipulation of large amounts of data, as is the case here.

The version of PATSTAT Global we are working with has 108,754,877 patent applications, collected in the table TLS201_APPLN, with information on 27 fields per application. After removing those applications that do not type A or T, the practical applications become 79,965,853. In addition, to facilitate the data processing, we will eliminate those fields that are not interesting to the study, so we reduce the table to only four fields (APPLN_ID, APPLN_AUTH, EARLIEST_FILING_YEAR, NB_INVENTORS).

Table TLS207_PERSON_APPLN has 276,448,369 relationships between persons and applications. We are left only with 193,723,106 relationships with inventors, which have a value in the field "NVT_SEQ_NR" other than 0.

We also reduce the table with information on persons (TLS206_PERSON), as only two fields are relevant to the study (PERSON_ID, PERSON_CTRY_CODE).

To perform the analysis, we link table TLS207_PERSON_APPLN to TRL TLS206_PERSON via the "PERSON_ID" field and table TLS201_APPLN to TLS207_PERSON_APPLN via the "APPLN_ID" field. Due to their low representativeness, we have discarded those years with less than 5,000 applications and eliminated applications without year information. The first year above the threshold we have set is 1893. To interpret the results, we have grouped them in the first years by decades and from 1971 onwards by five-year periods. The information for 2020 was incomplete when the PATSTAT edition was launched.

During processing, we will distinguish applications with country information for all inventors, applications without inventor or inventors' country information and "vague" applications, which are those with country information for some but not all inventors. Vague applications may be relevant for some studies, e.g. related to international cooperation if they have information on inventors from two or more countries. We will also calculate the percentage of applications with complete inventors' country information.

4 Results

Tables 1 and 2 show the more relevant results obtained for the first and the last period of analysis. We notice a large variability in the ratio of applications with complete inventors' country information/total applications, depending on the period and the filing authority. As expected, we can see considerable growth in the number of applications over the years, except for Great Britain (GB). This is attributable to the fact that protection is sought in the UK in many European Patent (EP) applications, not being GB one of the offices that assign a new national number to EP applications (DE, AT, ES, EE, SK and GR).

Table 1. Analysis of the information available on national patent applications by country with more than 1,000 patent applications in the period 1893-1900

Authority	Applications	With.country	No.country	Vague
GB	188482	45083	142304	1095
US	63246	61030	2046	170
CA	41534	20670	20860	4
CH	33381	16656	16719	6
AT	16436	1100	15272	64
ES	12502	0	12502	0
DE	2221	153	2068	0
FR	1602	517	1085	0

Moreover, taking into account that patent indicator analyses are usually done by year and technological field, we conclude that during the first periods, we will

find few offices that are interesting. For example, the Swiss office (CH) is the only interesting one in the period 1931-1940, with 115,620 applications, of which 68,225 have complete information on the country of the inventors.

Table 2. Analysis of the information available on national patent applications by country with more than 100,000 patent applications in the period 2011-2020

Authority	Applications	With.country	No.country	Vague
CN	3661993	180	3661827	14
US	1930870	1877783	53339	252
JP	1630056	69	1629993	6
KR	907421	732438	175501	518
EP	764991	723495	41663	167
DE	302927	276869	26076	18
TW	239415	234779	4653	17
RU	200442	157733	42738	29
CA	182714	182405	372	63
AU	163820	106	163715	1
GB	116099	59700	56408	9
BR	113547	100300	13284	37

Figure 1 presents applications by period of the ten authorities with more applications in the period from 2011 to 2020. We can see that the database has a significant number of applications to the US office for all periods. The German office has relevant records from the period 1921-1930. Records of the Canadian office are important in the first three periods and from 1971-1980. European patent applications started to become noticeable from 1971-1980 onwards. Finally, the Asian countries (JP, CN, KR, TW) started to become notable from 1961-1970 and took over the position of the office with the most applications registered in the database from 1971-1980.

More relevant is Figure 2, which shows the percentage of applications with complete inventors' country information by period for the ten authorities with the most applications in the period from 2011 to 2020. Given that the distribution of applications without information on the inventors' country might not be random and introduce some bias, very high percentages of applications that include the country of all inventors are of interest, e.g. over 90%. In the specific case of these ten countries, there is a considerable span between 1910 and 1970 that we can directly discard because of their low percentages. In the first two periods, only the applications to the US office would be of interest, especially those between 1901 and 1910, as this is a period with a high number of applications. The Canadian office shows outstanding values of more than 99% from 1991 onwards. Although not as remarkable, Germany and the United States also have excellent percentages in the same period. As far as the Asian offices are concerned, China (CN) from 1991 to 2000 and Chinese Taipei (TW) from 2001 are significant. Applications to the Russian Federation office are only of interest

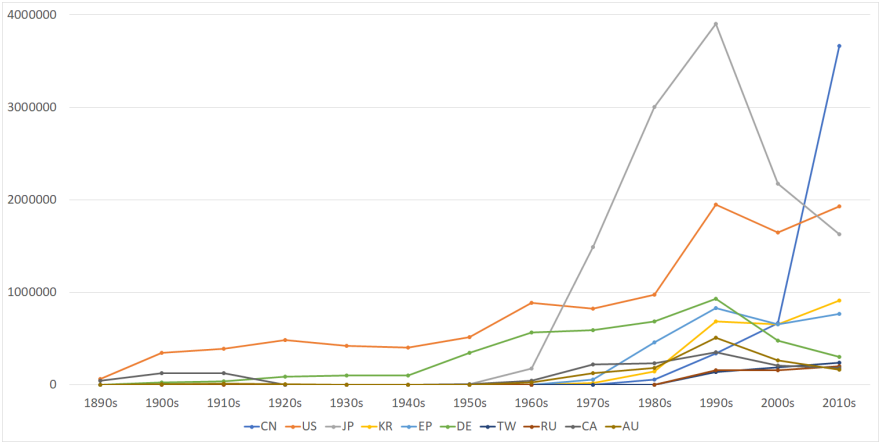

Fig. 1. Applications by period of the 10 authorities with more applications in the last period

in the 1980s. EP applications always maintain high percentages, being of great interest from their take-off in the 1980s onwards. However, we may be introducing a bias when using EP data, as these applications covering protection in several countries are more expensive and, therefore, would not usually include inventions from which a limited economic return is expected.

Figure 3 shows the evolution of applications and applications with complete inventors' country information by period for the six authorities with more applications from 2011 to 2020. The decades that are interesting for inventors' country studies are those with a high number of applications and a number of applications with complete inventors' country information very close to this.

5 Conclusions

When calculating indicators based on patents that take into account the field of the inventor's country, we have to be very careful when selecting both the filing authority and the period of years, as there is significant variability in the data available for the inventor's country field. In this analysis, we have grouped the data by decades. We have shown only those patent offices with the most applications in recent years, allowing us to identify the most relevant filing authorities and periods for this type of study. A more exhaustive analysis by annual periods rather than by decades would allow us to set much more precise intervals, with ratios of applications with complete inventors' country information/total applications close to one, which would further reduce the likelihood of biases appearing.

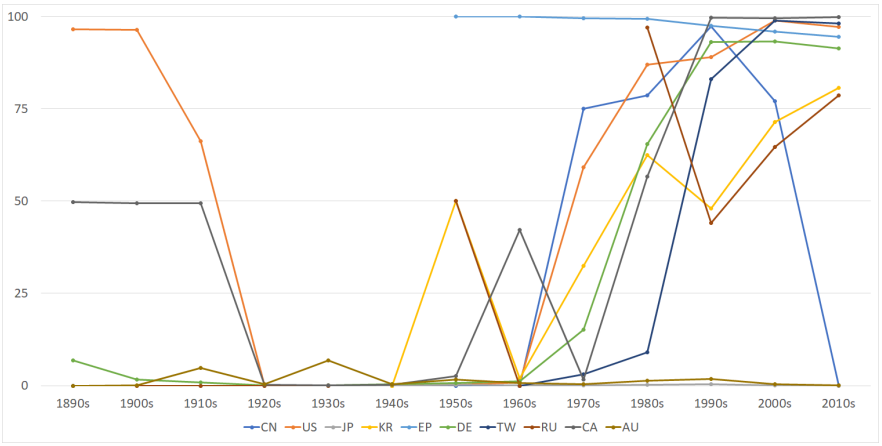

Fig. 2. Percentage of applications with complete inventors' country information by period of the 10 authorities with more applications in the last period

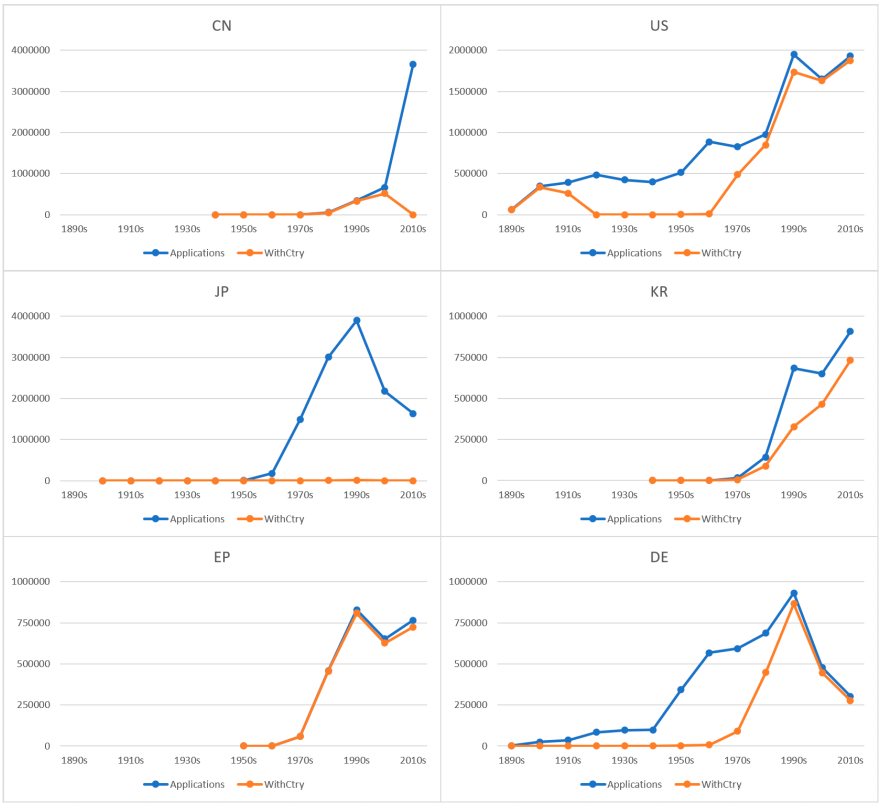

Fig. 3. Applications and applications with complete inventors' country information by period for the 6 authorities with more applications in the last period

References

[1] Yamada, H.: Identification methods and indicators of important patents. Library Hi TechVolume 40 (3), 750 – 785 (2022)

[2] Higham, K., De Rassenfosse, G., Jaffe, A.B.: Patent quality: towards a systematic framework for analysis and measurement. Res. Policy 50 (4), 104215 (2021)

[3] Zhai, Z., Ghosal, V.: Internationalization of innovation and firm performance in the pharmaceutical industry. International Review of Economics & Finance 80, 882-905 (2022)

[4] Huang, Z., Chen, H., Yip, A. et al.: Longitudinal Patent Analysis for Nanoscale Science and Engineering: Country, Institution and Technology Field. Journal of Nanoparticle Research 5, 333–363 (2003)

[5] De Prato, G., Nepelski, D.: Global technological collaboration network: network analysis of international co-inventions. J Technol Transf 39, 358–375 (2014)

[6] Ferrucci, E., Lissoni, F.: Foreign inventors in Europe and the United States: Diversity and Patent Quality, Research Policy 48 (9), 103774 (2019)

[7] European Commission: COMMUNICATION FROM THE COMMISSION TO THE EUROPEAN PARLIAMENT, THE COUNCIL, THE EUROPEAN ECONOMIC AND SOCIAL COMMITTEE AND THE COMMITTEE OF THE REGIONS on the Global Approach to Research and Innovation Europe's strategy for international cooperation in a changing world. COM/2021/252 final

[8] Harhoff, D., Scherer, F. M., Vopel, K.: Citations, Family Size, Opposition and the Value of Patent Rights. Research Policy 32(8), 1343-1363 (2003)

Seasonal variations of electrical signals of Pinus halepensis Mill. in Mediterranean forests in dependence on climatic conditions.

Rodolfo Zapata[1], Jose-Vicente Oliver-Villanueva[1], Lenin-Guillermo Lemus-Zúñiga[1], David Fuente[1], Miguel A. Mateo Pla[1], Jorge E. Luzuriaga[1] and Juan Carlos Moreno Esteve[2]

[1] ITACA - Institute of Information and Communication Technologies, Universitat Politècnica de València, València (Spain).
[2] Applied Physics Department, Universitat Politècnica de València, València (Spain)

Abstract. The temporal evolution of the electrical signal generated by Pinus halepensis was measured in a sample of 15 trees. Weekly experiments were carried out during a long-term campaign lasting over a year, while trials with a high frequency of measurements were also performed during several days. In the latter case, day-night oscillations of the electrical magnitudes were observed. Additionally, punctual meteorological events such as rainfall and electrical storms affect the electrical signal as well. The measured electrical intensity grows exponentially with the voltage. In general, higher electrical signals were gathered during the rainy seasons with moderate temperatures; while very low signals, including few measures of zero intensity, were obtained during the most stressful periods over the year, mainly by mid-summer. There is a strong correlation between the rainfall and the electrical signal. The rain-intensity correlation, together with sustained intensity values during the reproductive period in spring, suggests that this electrical magnitude could be an indicator of the physiological state of the tree and thus used for in situ and minimally invasive forest monitoring.

1 Introduction

The Mediterranean climate has never been benign for most tree species due to its long drought periods, torrential rains and extreme temperatures in summer [1], which facilitate bushfire ignition [2]. However, many plants have adapted to these conditions and supported the establishment of ecosystems with a great biodiversity [3].
In the current framework of climate change, Mediterranean climate areas are vulnerable to a decrease in precipitation, a plausible scenario over the next few decades, as the atmospheric circulation models predict [4]. This is a global challenge because these regions (Australia, Southern Africa, Chile, California and the Mediterranean basin) are present in every continent and they are densely populated.
According to Gracia [4], a rainfall reduction of 10% is expected in the Iberian Peninsula over the upcoming 50 years, as well as a decrease of 25% of soil's water content. Reduction in the soil's water reserve is a consequence of the increase in the rate of

C.Fernandez-Llatas and M.Guillen (Ed.):
Workshop on Innovation on
Information and Communication Technologies
(ITACA-WIICT 2022)

ISBN 978-84-09-46075-5

trees' transpiration during the vegetative period and the greater evaporative demand of the atmosphere [4]. The phytosanitary status of trees in Mediterranean climate zones is associated both with the characteristic climate fluctuations and with other ecological processes [5] such as outbreaks of fire [6]. In a climate change context, bushfire recurrence is enhanced in terms of intensity and frequency [5] by the temporary weakness of many trees [7]. Therefore, the early detection of weakened trees that do not display visible symptoms of disease yet, could represent a significant advancement in the planning of forest health management [5].

Remarkably, the existence of a continuous electrical potential between the electrodes inserted in the tree's phloem and the surrounding soil was discovered [8]. Additionally, it was recently documented that different environmental stimuli also produce electrical signal changes [9]. Further, according to some authors [10-15] the variation of electrical signals in response to the stimulus depends on the intensity of the stimulation.

This behaviour has been studied by other authors in research laboratories under controlled conditions [13-16]. This characteristic of the electrical signals could be used as an element for monitoring the state of the trees inside their ecosystem under natural conditions. Despite the different investigations carried out, it still remains unclear which environmental factors have the greatest influence on the tree's electrical signals. Few published works have studied the electrical signals of trees in controlled conditions and only for continental and Central European climatic areas, e.g., Aesculus hippocastanum [17] and Populus nigra [12] both in France, Salix alba in Austria [18], Quercus spp. and Fagus sylvatica [19,20]. Thus, to the best of our knowledge, any prior research which has addressed this topic under field conditions neither studied the electrical response of trees located in highly vulnerable ecosystems to climate change such as Mediterranean forests.

Fritts [21] affirms that trees growing in extreme conditions, such as Mediterranean ecosystems, respond more clearly to climatic variations. Consequently, the Aleppo pine (Pinus halepensis Mill.) is an interesting species for monitoring environmental changes because it is very well adapted to drought and its growth is highly related to the water supply [22]. In addition, Pinus halepensis is a pioneer species that is expanding strongly on the two banks of the Mediterranean basin [23] due to its high potential for natural regeneration after bushfires and also due to its ability to rapidly colonise abandoned agricultural lands [24].

In summary, the current and voltage values rely on the tree's physiological state [25-30] and thus, both electrical signal components could be robust indicators of the forest health under different environmental conditions and consequent vulnerabilities: growth potential, hydric stress, bushfire risk and pests, among others.

In a previous study, we analysed the most significant static factors influencing Pinus halepensis populations [31], i.e. experiments carried out for a short period of time at stable climatic conditions. We observed that the tree age significantly influences the measured electrical potential, obtaining higher values in young trees. Furthermore, we conclude that the amplitude of the electrical signals does not depend on the location of the electrode. Both components of the electrical signal (the potential difference and the ISC) are constant, regardless of the orientation and height at which the measurement electrode is inserted into the tree.

Based on this acquired knowledge, the aim of this research is to analyse the temporal evolution of the electrical signal of a representative group of Pinus halepensis in Mediterranean forest. Indeed, this is the first study researching the electrical behaviour of a representative sample of trees in natural conditions and it is also pioneering in measuring the electric intensity generated by a tree. The chosen pine is a paradigmatic Mediterranean species that quickly responds to climatic variations, and hence, it is a representative object of research. Regarding the experimental planning, the electrical measurements with a higher sample frequency were carried out for a period of several days, while the long-term trials were performed for a campaign lasting more than one year. In summary, the main objective of this work is to detect and analyse the seasonal but also day-night variations of electrical signals of Pinus halepensis in a Mediterranean ecosystem.

2 Material and Methods

Both components of the electrical signal, voltage and current [32], were measured in two different data acquisition experiments, one for short, the other for long periods. In the first trial, data were recorded with a weekly resolution to assess the electrical signal evolution throughout the annual vegetative cycle. In the other experimental set-up, signal values were obtained each minute over several consecutive full days. In this way, we can observe the short-term changes in voltage and current along the day-night cycles in different stages of the pine vegetative cycle.

2.1 Selection of representative species and forest

As in our previous work [31], Pinus halepensis is the selected arboreal species on which the measurement of the electrical signals has been carried out because it is a representative coniferous, native to the Mediterranean region and present in almost all regions of both banks of the Mediterranean basin [33, 36-41]. Moreover, Pinus halepensis presents clear relationships between growth and climatic variables. Thus, it is a reliable species for dendroclimatological studies [22]. Different studies for the Iberian Peninsula [34,35] suggest that the growth series reflect a strong influence of climatic factors, with a higher sensitivity than that observed in other Pinus species such as Pinus sylvestris, Pinus nigra, Pinus pinaster and Pinus mugo. Thus, understanding the impact of different environmental factors on the electrical response of this species may be of interest to the scientific community [22].

In our previous work, it was found that the amplitude of the signal is significantly greater in younger trees than in mature ones [31]. For this reason and to facilitate the measurement of the electrical signal, it was decided to look for a forest that had enough young trees within an area not affected by significant environmental disturbances such as recent bushfires, pests or damage due to heavy snowfall. Therefore, we decided to use a natural regenerated forest located within the protected area of the

Sierra Calderona Natural Park in the Region of Valencia, Spain. The selected sample stand has an approximate size of 0.25 hectares and is located at latitude 39° 45′ 28.80" N and longitude 0° 30′ 36.36" W. The age of the trees is in average 27 years. The mean breast height diameter is 12.10 cm and the mean height 5.16 m. The stock density is 484 trees/ha.

2.2 Electrodes

Two model electrodes were used according to their function, a stainless steel for the tree and a platinum-iridium for the ground [12,16,31,42,43]. We inserted the stainless-steel electrode directly at 1.5 m above the ground into the trunk to be in contact with the phloematic tissue. We chose stainless steel screws as electrodes because they can be easily inserted and removed from trees, causing only a minor wound. Additionally, the screws have a greater contact surface with respect to the smooth electrodes due to their thread. The contact with the phloematic tissue was ensured by inserting the electrodes with a torque wrench that allowed us to detect the change in hardness of the tissue and to cross the phloematic tissue. The latter action is fundamental since electrical signals are transmitted more easily along this tissue, given its lower resistance to electrical flow, compared to other plant tissues [9].

The second type of electrode was a non-polarization titanium-nitride-coated platinum-iridium alloy electrode (1999/5/EC) [44] and was used as ground reference. Due to the hardness of the soil, this electrode was buried 15 cm in the mineral soil, discarding the centimetres of topsoil, at a minimum distance of 3 m from the tree.

Both electrodes were connected with the measuring equipment through an electrical connector and a 0.5 mm copper conductor cable insulated with a flexible plastic coating (CE 0123).

2.3 Measures for the long-term evolution

The long-term experimental design was based on the knowledge acquired for individual hardwoods [10,12,19] and on our previous experience with Pinus halepensis [31]. This trial aims to observe the electrical signal evolution within the group of selected pines throughout their annual vegetative cycle.

2.3.1 Procedure

Voltage (V) and short-circuit current (ISC) data were collected at the same solar time once every Monday for 16 months, between May 28th 2018 and September 30th 2019, comprising more than a complete vegetative cycle. Four values (one for each cardinal point) of each component of the electrical signal and for each of the 15 representative specimens of the study population were recorded, i.e., 60 measurements every week.

2.3.2 Measurement equipment and external data sources

Voltage and current values were measured with a UT71D UNI-T multimeter with an input impedance of 2.5 GΩ and an accuracy of 0.1% ± 2 millivolts (mV).

Meteorological data of the area were provided by a professional weather station installed in 39° 46' 10.12" N, 00° 31' 14.19" W, located very close to the research plot. The weather station is a Davis Vantage VUE model owned by the Valencian Association of Meteorology 'Josep Peinado' (AVAMET) [45]. The meteorological variables to be correlated with the electrical signal components are the temperature, relative air humidity, atmospheric pressure, wind speed and precipitation. For simplicity, the daily mean of the collection day was used. For the rainfall amount, the accumulated weekly precipitation was assumed.

2.3.3 Trees selection

15 trees of a forest population of Pinus halepensis were selected following the method described by Hapla and Saborowski for sampling representative trees in a forest stand [46]. In this way, the tree selection can be considered as a representative sample of the surrounding forest. This methodology has been verified in different studies related to the characteristics of trees and the physical properties of wood [47-53].

2.3.4 Statistical Analysis

The Spearman correlation coefficient was used to link the voltage and intensity data with the meteorological variables. The use of Spearman correlation was based on other works [54, 55] affirming that this coefficient is less sensitive than other statistics to outliers.

2.4 Measures for short-term evolution

This experiment monitors the influence of the day-night cycles on the electrical signal in a single tree as described in [19, 42, 56, 57]. Voltage and current measurements were prolonged for several days in a row, and the recording sessions took place in different seasons to observe electrical variations throughout the year.

2.4.1 Procedure

The electrical potential difference was registered every second, while the intensity was measured during ten seconds every two minutes to allow the electrical signal to recover. Table 1 shows the dates on which the 24-hour measurement sessions were carried out.

The experiments carried out during 2019 only included voltage measures, while intensity and voltage were both measured from 2020 onwards (see Table 1).

Cam-paign ID	Dates	D ays	Season	Measure-ment
1	26th April to 1st May, 2019	6	Spring	Voltage
2	29th June to 3rd July, 2019	5	Summer	Voltage
3	15th June to 20th June, 2020	6	Spring	V + ISC
4	6th March to 12th March, 2021	6	Winter	V + ISC

Table 1. Short-term experiment calendar

2.4.2 Measurement equipment and external data sources

Figure 2 shows the position of the equipment for data measurement on the selected tree. In this figure you can also see the installation in height on the trunk to protect the action of the fauna the watertight capsule that, in turn, protects the electronic components of measurement from meteorological factors.

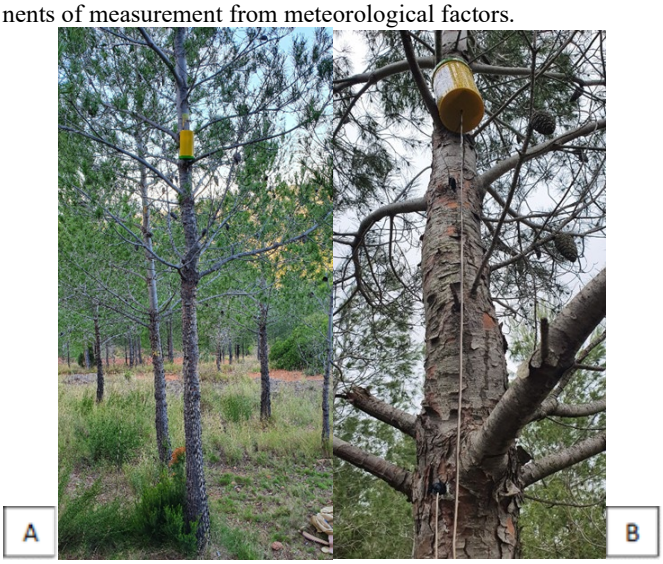

Figure 2. Short-term data-acquisition emplacement in a selected tree. Overview of the installation (A).Close vision of the watertight capsule (B).

For the short-term data-acquisition campaign, a prototype was developed that uses a Mooshim Mooshimeter BLE-DMM-2X-01 device with an accuracy of 0.5% for any

voltage measurement. The intensity magnitude was gathered by measuring the voltage drop across a shunt.
The intensity of the electrical signal dropped to values close to zero if the measurement device was maintained connected through the shunt, as our prior experience indicates (see Figure 3). To avoid the plant stress emerging from the shunt experiment, the prototype had a relay controlled with an automatic programmable system (Pycom). In this way, the circuit could periodically be interrupted, making current measurements through the shunt punctually and not continuously.
Sunrise and sunset hours were consulted in the Spanish National Astronomical Observatory[58].

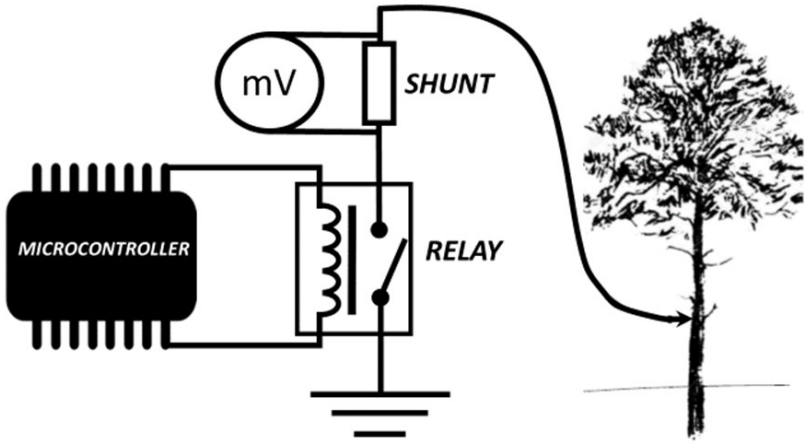

Figure 3. Circuit diagram of measurement through the shunt

2.4.3 Tree selection
For the 24-hour monitoring, it was necessary to work on a single tree due to equipment availability limitations. The selected tree (number 11) for the continuous evaluation displayed a yearly average voltage that was the closest to the group's mean among all specimens of the long-term data collection.

3 Results

3.1 Long-term evolution

The first obtained results are the voltage and intensity signals for the long-term experiment. Figure 4 shows the mean, maximum and minimum values for the population

sampled during the 16-month campaign. The maximum recorded value is 1.10 V for the voltage (Figure 4a) and 11.05 µA for the current (Figure 4b), while the minimum magnitudes correspond to 0.11 V and 0.00 µA, respectively. It can be observed that the voltage values are maintained within a narrower range with respect to the electrical current. This means that there are smaller variations among the specimens for the voltage than for the current. The highest values were measured in October and November 2018 and April and May 2019, corresponding to autumn and spring seasons. Conversely, the minimum values were recorded in February, March 2018, July and August of both years. So, during winter and summer, minimal values are registered, especially for the summer months. The vertical dashed lines represent the dates on which the tree pictures were taken (Figure 4c). One photo was taken at the end of July, which corresponds to the period with the highest hydric stress for the tree. The second picture corresponds to the end of April, which is the beginning of the growth period, that is, when temperatures are not too high, and there is enough water availability due to intense rainfalls in the spring.

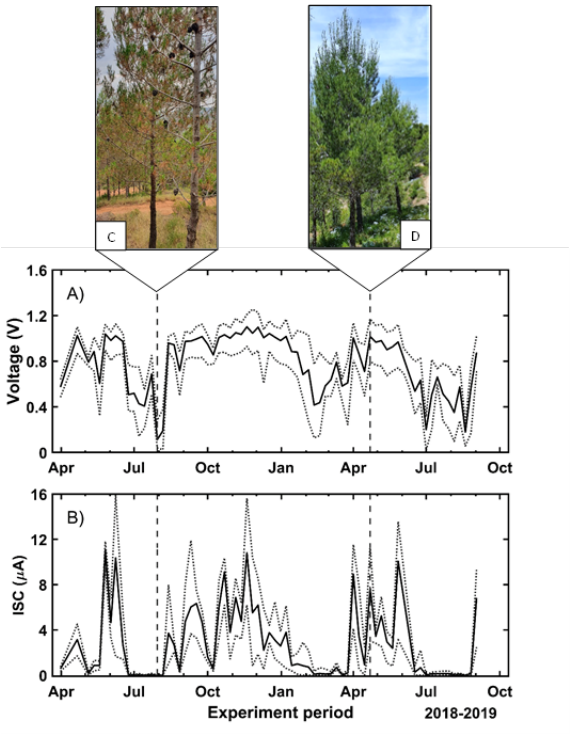

Figure 1. Temporal evolution of the voltage (a) and the ISC (b) during the long-term experiment given as the principal value of all trees. Maximum and minimum values are also depicted (dotted). Dashed vertical lines represent the dates when the tree pictures (C/D) were measured.

Figure 5 shows the mean voltage and intensity values of all trees along with the long-term experiment. Here, we can observe that there is a characteristic relationship between both magnitudes. Remarkably, voltages below 0.6 V do not allow any measurable ISC values. These records are only gathered during summer seasons and in the coldest months of the year. Alternatively, high voltage and ISC figures are gathered during both rainy seasons under moderate temperatures. The relationship between both electrical components follows an exponential behaviour. In fact, voltage increases above 1.0 V promote considerable ISC rises, Which represents a consistently recurring phenomenon throughout the study period.

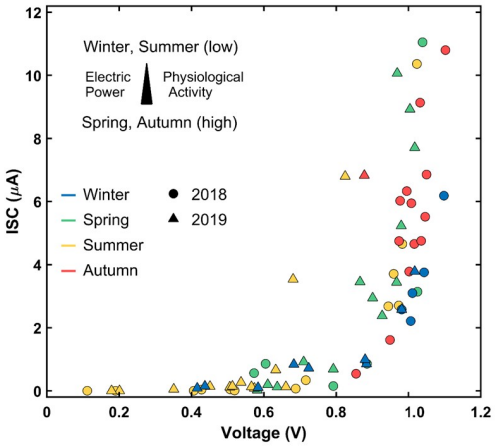

Figure 5. Relationship between the mean voltage and ISC of all trees for the long-term campaign

3.2 Relationship between the electrical signal and the atmospheric variables

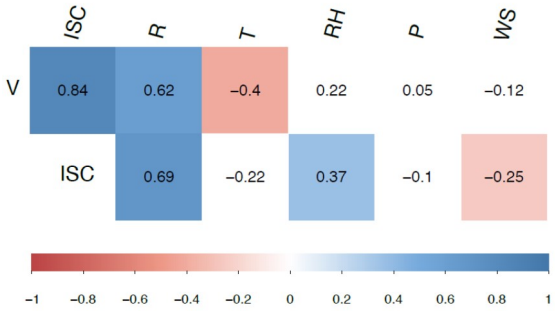

Figure 6. Result of Spearman's correlation. Values within a coloured box correspond to a statistically significant correlation different from 0 with the alpha significance level equal to 0.05.

Figure 6 shows the main results obtained from Spearman's correlation analysis. Based on its outcome, it can be stated that there is a strong positive correlation between the voltage and the ISC values, as previously described. This correlation reaches a Spearman □-value of 0.838 with $p < 0.05$. Nevertheless, there is no correlation between the voltage, nor the ISC, and the atmospheric pressure. In relation to the wind speed and the relative humidity, there is neither a significant correlation of these variables with the voltage variable since the calculated p-values are 0.372 and 0.082, respectively. Analogously, the effect of the wind on the ISC (negative effect) is statistically significant. However, this is not the case for the ISC and the air humidity. Moreover, the relationship with the daily temperature was shown to be significant only with respect to the voltage, being such an influence negative with □ = -0.402. In contrast, there was no correlation with statistical significance for the ISC magnitude, being the associated $p = 0.083$.

The precipitation amount is the atmospheric variable showing the highest correlation according to the Spearman methodology. There is a statistically significant correlation for both, the voltage and the ISC, with a $p < 0.05$ and reaching a □□value of 0.652 for the voltage and 0.709 for the ISC. Since rainfall is the most influential variable on the tree's electrical signals, we will now plot the weekly accumulated precipitation on the voltage and ISC evolution as depicted in Figure 7. It can be observed that while the voltage seems to be less dependent on the precipitation, this is not the case for the ISC values. Thus, this magnitude is correlated with the rain intensity. Indeed, ISC increases are measured when it had rained the week before. To some extent, the intensity rise seems to be proportional to the rainfall amount for summer and autumn, whereas there is no recorded rain in winter during our experiment period. However, the trees in spring seem to strongly react to the rain regardless of its intensity.

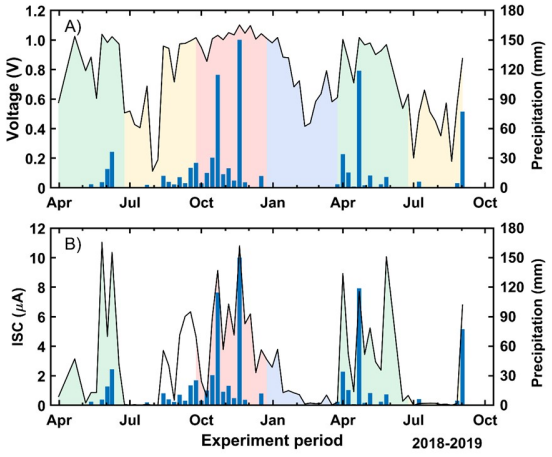

Figure 7. Temporal evolution of the voltage (A) and the ISC (B) during the long-term experiment given as the mean value of all trees. The rainfall amount is also displayed. Background colours represent the corresponding astronomical season**.**

3.3 Short-term evolution

Four 24-hour experiments were carried out during several days at different seasons to observe the trees' electrical response to the day-night cycles. The graph for each voltage experiment is displayed in Figure 9. Similarly, the concurrent ISC trials (only two experiments in this case) are shown in Figure 10.

The first trial was performed from 26th April to 01st May 2019. That is, during the most important growing period of the trees due to their vegetative activity [67]. The maximum temperature was 20.6°C and the experiment was carried out three days after the last precipitation (2.6 mm) and seven days since the last storm occurred (139.4 mm). Figure 9a shows the daily voltage variations, which account for 0.05 V. Moreover, the highest potential difference is gathered at night. Indeed, the largest difference is obtained at the local sunrise time. The electrical signal decrease gradually until reach a minimum voltage difference at the zenith. From this moment on, the registered potential difference begins to increase until the sunset.

The next test was carried out from 29th June to 4th July 2019 (Figure 9b). The trees in this period are in one of the most stressful phases of the year due to the high temperatures and scarce water availability. Measurements were taken 37 days after the last recorded storm, with a maximum temperature measured by the meteorological station of 36.9°C. Under these conditions of water stress, the signals continue to show daily oscillations of 0.05 V and an inversion of the periods of maximum and minimum voltage compared to the spring period. There is a steep voltage reduction for the period between 9:30 p.m. and 10:00 a.m. of the next day. Later, there is a relatively moderate voltage increase between 10:00 a.m. and 2:00 p.m. Then, a stability period is reached until approximately 8:30 p.m. to end up with a marked decrease until approximately 9:30 p.m., when the cycle begins again.

Other measurement series were made during the period between the 15th and the 20th of June 2020 (Figure 9c). With an elapsed period of five days since the last period of rainfall, when 10.6 mm were collected in three days of rain. In this period, the weather station recorded a maximum temperatures of 26.6°C. The graph shows no apparent variations between night and day hours. On June 19th, we observe a marked electrical anomaly of more than 1 V that coincides in date and time with an electrical storm with hardly any measurable rain (0.6mm) over the tree area. The sudden increase of voltage disappeared few hours after the storm had vanished. Figure 9c also outlines a clear downward trend in the voltage values along the studied period.

Furthermore, between the 6th and the 12th of March 2021, the maximum recorded temperature was 22.1°C, while the minimum accounted for 2°C. During this measurement period, an overall rainfall of 21.4 mm was recorded on the 7th and the 8th of March, in this case without any atmospheric electrical activity. This rain event coincides with a sudden increase in the registered electric signal amplitude as shown in Figure 9d. Unlike the transitory voltage behaviour displayed in Figure 9c, the electrical signal does not return to the previous level it held before the precipitation occurred (0.4 V). On the contrary, after the rain episode, a voltage magnitude of 0.6 V is maintained for almost two days. Then, it slowly decreases up to values close to 0.5 V.

During the last two voltage experiments, ISC measurements were also gathered. The related results are displayed in Figure 10. The experiment carried out in June

2020 (Figure 10a) shows the trend of the ISC along the studied period. It can be seen that its evolution resembles the voltage progress, including the electric anomaly derived from the storm. Unlike the voltage trend, the ISC shows clear maximum and minimum values, corresponding to midday and some hours after midnight, respectively. In this case, a voltage level of 0.4 V is enough to sustain some current. However, its magnitude is close to zero. Similarly, the ISC measurements gathered during the second week of March 2021 (Figure 10b) display the same voltage trend of that week: after the rain event, the ISC and the voltage remain much higher than before the rainfall. In particular, the initial current level of 0.4 μA is multiplied by a factor of 10 after the rain and slowly decrease at a rate of 1 μA each two days approximately. In this case, no clear local extrema are distinguishable during this week. This means that the surplus of electricity derived from the intense rain masks the daily electrical oscillations.

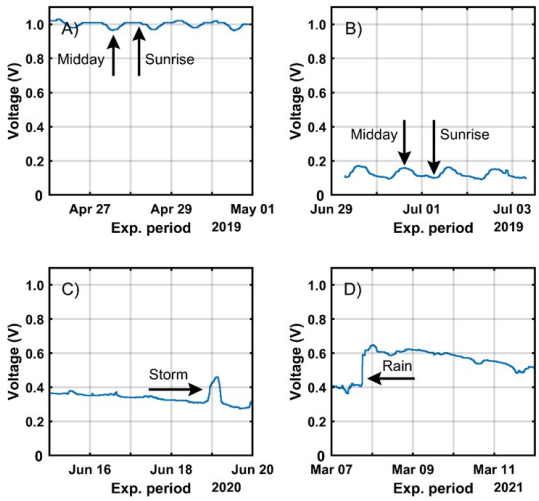

Figure 9. Voltage evolution for different short-term experiments. Events related with voltage changes are indicated with arrows. A) from 26th April to 1st May 2019. B) from 29th June to 4th July 2019. C) from 15th to 20th June 2020. D) from 6th to 12th March 2021.

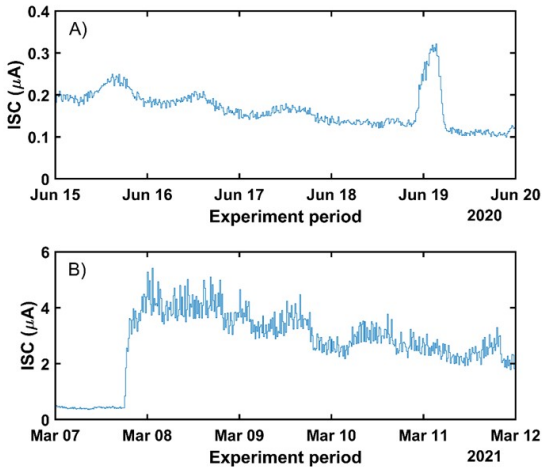

Figure 10. ISC evolution during two different short-term experiments. ISC evolution (A) and (B) correspond to the experiment shown in (C) and (D) of Figure 9, respectively.

4 Discussion

4.1 Long-term evolution

The long-term evolution of the voltage and the ISC in the trees is strongly affected by the seasonal characteristics of the Mediterranean climate: low and occasionally zero electrical signals are collected during dry periods, that is, in winter and especially in the middle of summer as shown in Figure 4. In this sense, the hydric stress suffered by the trees during these periods leads to yellow colouration and a lower needle density [59]. This contrasts sharply with the intense green colour and the higher needle density displayed by the pines in autumn and spring, as shown in Figures 4C and 4D when both electrical components are at their maximum values. Prior literature also reports seasonal variations of the voltage in trees under controlled conditions over long periods [12,19,56]. However, extreme values might be obtained in different periods according to the climatic characteristics of each location and consequently to the adaptation of each tree species to the environmental conditions of its habitat.

In this research, voltages below 0.6 V do not support any measurable ISC values. These records are normally gathered during the summer season and in the coldest months of the year. Thus, we expect the tree to stay in a dormant state when such magnitudes are measured. In addition, the rainfall seems to be strongly correlated

with the ISC magnitude throughout the year, with the only exception of the spring months. During this period, sustained ISC values are measured regardless of the precipitations. Certainly, it is known that Pinus halepensis presents marked seasonally growth periods [60] due to the climatic pattern along the year, concentrating its main physiological activity in spring when water availability is high and temperatures are in the optimal range. Alternatively, Pinus halepensis stops growing during the summer and winter. Moreover, it is known that the lack of water leads to the interruption of plant growth in many species, including this Mediterranean pine [59]. We similarly demonstrate that the electrical signal, especially the intensity, shows a reduction in the periods when the water availability is scarce. Hence, we expect the ISC magnitude to be a good indicator of the physiological state of the tree and that values below the given voltage threshold correspond to null net photosynthetic activity. Moreover, Gil et al. [14] found that the voltage values gathered in avocado trees under controlled conditions were dependent on changes in the soil water content.

In addition, some authors have identified a seasonally differentiated effect of the temperature on the radial growth of Pinus halepensis [60]. They reported a negative relationship in the months of July to October and a positive one during the first semester of the year. We have also detected such a bimodal trend in our results: during the first half of the year, there is a positive correlation between the temperature and the voltage, while it is negative in the second half. Hence, considering the growth-temperature dependence described in [60], it might be possible to establish a correlation between the pine growth and the voltage.

Another outcome of this research is the analysis of the electrical signal of individual trees. The individual measurements confirm that all trees experience similar trends regarding their electrical output. However, there is some signal variability, especially in the intensity magnitude (Figure 4b) and to a lesser extent in the voltage (Figure 4a), despite being all specimens coeval and located in a plot with similar soil characteristics. Similarly, minor differences could also be appreciated among the trees regarding their external aspects and the harsh periods regarding extreme climatic conditions. The dissimilarities among the specimens could be a consequence of the microgeology around each tree. Indeed, minor local differences in the soil and subsoil properties can also affect the tree response [61]. Furthermore, other authors mention that the influence of microsites [62] and the morphological attributes of each tree [63] can confer unique characteristics to each specimen and thus, a partially different electrical response might emerge in each tree.

4.2 Short-term evolution

The appearance of daily cyclical variations of the electrical response coincides with the experiences reported by other authors [42,56]. Figure 9a displays voltage oscillations, whose mean value is close to 1 V. The signal range, i.e., the maximum and minimum value difference is around 30 mV. This figure is very close to that published by Koppán [56], who measured daily voltage variations in Quercus cerris during the same week of the year and also reported maximum values at night and minimal during midday. Alternatively, daily variations during summer display an inversion (Figure 9b) with respect to the time of local extreme appearance in spring (Figure

9a): minimal voltage values are gathered at night and the highest measurements are obtained during the day in the hot period.

During two of our short-term trials, two electrical anomalies originated by an electrical storm and a punctual rain were registered. In the first case, a sudden and transient increase in the voltage and the ISC was detected (Figure 9c and Figure 10a). On the contrary, in the second case a signal enlargement was recorded that lasted longer than the atmospheric instability (Figure 9d and Figure 10b), probably due to a higher water availability in the soil. Hence, atmospheric events can also alter both electrical magnitudes and have to be taken into account when analysing short-term characteristics of the electrical signals in Mediterranean pines. Moreover, the ISC measurements describe the same behaviour as in the voltage case after the appearance of the mentioned electrical phenomena, as displayed in Figure 10a and Figure 10b. Similar electrical alterations were observed in [56], since the voltage maxima in Fagus sylvatica are enhanced when atmospheric electricity is present. Moreover, precipitation was found to impact the electrical outcome for several days as it occurs in our research.

Additionally, some authors have observed the reversal of the current flow in the trees due to the presence of positively charged atmospheric islands [57]. Nevertheless, we could not recognize such a phenomenon in our measurements.

In summary, we have identified the existence of seasonal and daily patterns of both electrical-signal components of Pinus halepensis in natural ecosystems. In addition, we have also found a clear correlation between the fallen precipitation on the area and the variations in the electrical signal of the trees, especially with respect to the electrical intensity. Remarkably, we found a minimum voltage of 0.6 V that is necessary to measure intensity flows in our circuit. Since lower voltage values are only measured during the most demanding periods of the year, that is, when the pines have a very low photosynthetic activity, we think that the ISC could be a good estimator of the physiological activity. Moreover, soil humidity is the most limiting factor for pine growth in the Mediterranean ecosystem and periods without rain are clearly correlated with low voltages and zero ISC measurements. So, the measured electrical components seem to be potential estimators of the tree health and activity, e.g. monitoring moisture content and consequently, bushfire or pest risk.

Further work is necessary to predict the contribution of each atmospheric and environmental factor to the electrical signal. Indeed, a complete understanding of the electrophysiological behaviour of Pinus halepensis is critical for future applications such as bushfire risk or pest monitoring and detection. Hence, the electrical signals generated by the trees could be used as indicators of the tree physiological state and thus, leveraged for in situ and permanent monitoring of Mediterranean forests in the actual scenario of climate change.

References

1. Gimeno, T. E., Pías, B., Lemos-Filho, J. P., & Valladares, F. (2009). Plasticity and stress tolerance override local adaptation in the responses of Mediterranean holm oak seedlings to drought and cold. Tree Physiology, 29(1), 87-98.
2. Pausas, J. G., & Vallejo, V. R. (1999). The role of fire in European Mediterranean ecosystems. In Remote sensing of large wildfires (pp. 3-16). Springer, Berlin, Heidelberg.
3. Syphard, A. D., Radeloff, V. C., Hawbaker, T. J., & Stewart, S. I. (2009). Conservation threats due to human-caused increases in fire frequency in Mediterranean-climate ecosystems. Conservation Biology, 23(3), 758-769.
4. Gracia, C.A., Sabaté, S. y Sánchez, A. 2002. El cambio climático y la reducción de la reserva de agua en el bosque mediterráneo. Ecosistemas 2002/2 (URL:http//www.aeet.org/ecosistemas/022/investigacion4.htm)
5. Guillen-Climent, M.L., Mas, H., Fernández-Landa, A., Algeet-Abarquero, N., Tomé J.L. 2020. Using hipersepctral images for decay detection in Pinus halepensis (Mill.) in the Mediterranean forest. Revista de Teledetección, 55, 59-69. https://doi.org/10.4995/raet.2020.13289.
6. De Dios, V. R., Fischer, C., & Colinas, C. (2007). Climate change effects on Mediterranean forests and preventive measures. New forests, 33(1), 29-40.
7. Hódar, J. A., Zamora, R., & Cayuela, L. (2012). Climate change and the incidence of a forest pest in Mediterranean ecosystems: can the North Atlantic Oscillation be used as a predictor?. Climatic Change, 113(3-4), 699-711.
8. Love CJ, Zhang S, Mershin A. Source of sustained voltage difference between the xylem of a potted Ficus benjamina tree and its soil. PloS One. 2008;3:8.
9. Patricio Oyarce & Luis Gurovich (2010) Electrical signals in avocado trees, Plant Signaling & Behavior, 5:1, 34-41, DOI: 10.4161/psb.5.1.10157
10. Datta P, Palit P. Relationship between environmental factors and diurnal variation of bioelectric potentials of an intact jute plant. Curr Sci. 2004:87;680–683.
11. Gora EM, Yanoviak SP. Electrical properties of temperate forest trees: a review and quantitative comparison with vines. Can J For Res. 2015;45(3):236–245. doi:10.1139/cjfr-2014-0380.
12. Gibert D, Le Mouel JL, Lambs L, Nicollin F, Perrier F. Sap flow and daily electric potential variations in a tree trunk. Plant Sci. 2006;171 (5):572–584. doi:10.1016/j.plantsci.2006.06.012.
13. Gil PM, Gurovich L, Schaffer B. The electrical response of fruit trees to soil water availability and diurnal light-dark cycles. Plant Signal Behav. 2008;3(11):1026–1029. doi:10.4161/psb.6786.
14. Gil PM, Gurovich L, Schaffer B, Garcia N, Iturriaga R. Electrical signaling, stomatal conductance, ABA and ethylene content in avocado trees in response to root hypoxia. Plant Signal Behav. 2009;4(2):100–108. doi:10.4161/psb.4.2.7872.

15. Rios-Rojas L, Morales-Moraga D, Alcalde JA, Gurovich LA. Use of plant woody species electrical potential for irrigation scheduling. Plant Signal Behav. 2015;10(2):e976487. doi:10.4161/15592324.2014.976487.

16. Volkov AG, Ranatunga DRA. Plants as environmental biosensors. Plant Signal Behav. 2006;1:105–115.

17. Morat P, Le Mouel JL, Granier A. Electrical potential on a tree. A measurement of the sap flow? Comptes rendus de l'Academie des sciences Serie 3, Sciences de la vie. 1994;317:98–101.

18. Gindl W, Loppert HG, Wimmer R. Relationship between streaming potential and sap velocity in Salix Alba L. PHYTON-HORN-.1999;39:217–224.

19. Koppan A, Szarka L, Wesztergom V. Temporal variation of electrical signal recorded in a standing tree. Acta Geodaetica et Geophysica Hungarica. 1999;34:169–180.

20. Koppan A (2004). Variations of the natural electric potential differences occurring on tree trunks and their relationship with the xylem sap flow. PhD Thesis. University of West Hungary. Sopron,Hungary.

21. Lamb, H.H. and Gray, B.M. (1978), Tree rings and climate. By H. C. Fritts. London, New York and San Francisco, Academic Press, 1976. Q.J.R. Meteorol. Soc., 104: 236-237. doi:10.1002/qj.49710443923

22. Olivar, J., Bogino, S., & Spiecker, H. (2009, June). Influencia del clima en el crecimiento radial de Pinus halepensis de diferentes clases sociales e identificación de las variables climáticas más importantes. In Congresos Forestales.

23. Maestre, F. T., Cortina, J., Bautista, S., & Bellot, J. (2003). Does Pinus halepensis facilitate the establishment of shrubs in Mediterranean semi-arid afforestations?. Forest Ecology and Management, 176(1-3), 147-160.

24. Chomel, M., Fernandez, C., Bousquet-Mélou, A., Gers, C., Monnier, Y., Santonja, M., ... & Baldy, V. (2014). Secondary metabolites of P inus halepensis alter decomposer organisms and litter decomposition during afforestation of abandoned agricultural zones. Journal of Ecology, 102(2), 411-424.

25. Rathgeber, C. B., Cuny, H. E., & Fonti, P. (2016). Biological basis of tree-ring formation: a crash course. Frontiers in Plant Science, 7, 734.

26. Castagneri, D., Fonti, P., von Arx, G., & Carrer, M. (2017). How does climate influence xylem morphogenesis over the growing season? Insights from long-term intra-ring anatomy in Picea abies. Annals of botany, 119(6), 1011-1020.

27. Ekberg, Inger, Gösta Eriksson, and Ingegerd Dormling. "Photoperiodic reactions in conifer species." Ecography 2, no. 4 (1979): 255-263.

28. Mattsson, A. (1986). Seasonal variation in root growth capacity during cultivation of container grown Pinus sylvestris seedlings. Scandinavian Journal of Forest Research, 1(1-4), 473-482.

29. Rodríguez-Calcerrada, J., Salomón, R., & Gil, L. (2015). Transporte y reciclaje de CO2 en el interior del árbol: factores que complican la estimación de la respiración leñosa a través de la emisión radial de CO2. Bosque (Valdivia), 36(1), 5-14.

30. Pfanz, H., Aschan, G., Langenfeld-Heyser, R., Wittmann, C., & Loose, M. (2002). Ecology and ecophysiology of tree stems: corticular and wood photosynthesis. Naturwissenschaften, 89(4), 147-162.

31. Zapata, R., Oliver-Villanueva, J. V., Lemus-Zúñiga, L. G., Luzuriaga, J. E., Mateo Pla, M. A., & Urchueguía, J. F. (2020). Evaluation of electrical signals in pine

trees in a mediterranean forest ecosystem. Plant Signaling & Behavior, 15(10), DOI: 10.1080/15592324.2020.1795580.

32. The Editors of Encyclopaedia Britannica. Electric power. Encyclopædia Britannica. Encyclopædia Britannica, inc. Date Published: December 04, 2019. URL:https://www.britannica.com/technology/electric-power Access Date:August 31, 2020.

33. De Luis M, Čufar K, Di Filippo A, Novak K, Papadopoulos A, Piovesan G, Smith KT. Plasticity in dendroclimatic response across the distribution range of Aleppo pine (Pinus halepensis). PLoS One. 2013;8:12. doi:10.1371/journal.pone.0083550.

34. Richter, K., Eckstein, D., & Holmes, R. L. (1991). The dendrochronological signal of pine trees (Pinus spp.) in Spain.

35. Bogino, S. M., & Bravo, F. (2008). Growth response of Pinus pinaster Ait. to climatic variables in central Spanish forests. Annals of Forest Science, 65(5), 506-506.

36. AAVV. (2008). Distribution map of aleppo pine. EUFORGEN 2009,[Retrieved 2020 July 16]. www.euforgen.org

37. Fadi B, Semerci H, Vendramin GG. 2003. EUROFORGEN technical guidelines for genetic conservation and use for aleppo pine (Pinus halepensis) and brutia pine (Pinus brutia). IPGRI, International plant genetic resources institute. Rome (Italy). p. 6. ISBN 92-9043-571-2.

38. Mauri A, Di Leo M, de Rigo D, Caudullo G. 2016. Pinus halepensis and Pinus brutia in Europe: distribution, habitat, usage and threats. In: San-Miguel-Ayanz J, de Rigo D, Caudullo G, Houston Durrant T, Mauri A, editors. European Atlas of Forest TreeSpecies. Publ. Off. EU, Luxembourg. p. e0166b8+.

39. Pausas JG, Ribeiro E, Vallejo R. Post-fire regeneration variability of Pinus halepensis in the eastern Iberian Peninsula. For Ecol Manage. 2004;203(1–3):251–259. doi:10.1016/J. FORECO.2004.07.061.

40. IFN3. Tercer inventario forestal nacional (3rd National Forest Inventory of Spain). Ministerio para la Transformacion Ecologica y el Reto Demografico; Spain, 2007. [Retrieved 202 July 16] https:// www.miteco.gob.es/es/biodiversidad/servicios/banco-datosnaturaleza/informacion-disponible/ifn3.aspx

41. Valbuena, P., & Bravo, F. (2008). Stand density Management diagrams for two mediterranean pine species in Eastern Spain. Forest Systems, 17(2), 97-104.

42. Cardoso SS, Carrondo LB, Marques JM, Narciso PN, Rocha MJ, Rodrigues IN, Soares A. (2004). Monitorization of the electrical signal generated by a tree. February 2004 – 4th luso-spanish assembly on geodesy and geophysics.

43. Hao, Z., Li, W., & Hao, X. (2021). Variations of electric potential in the xylem of tree trunks associated with water content rhythms. Journal of Experimental Botany, 72(4), 1321-1335.

44. DIRECTIVE 1999/5/EC OF THE EUROPEAN PARLIAMENT AND OF THE COUNCIL of 9 March 1999.

45. Asociación Valenciana de Meteorología 'Josep Peinado' (AVAMET) URL:https://www.avamet.org/mx-mxo.php?id=c11m902e01. Access Date: December 15, 2020.

46. Hapla F, Saborowski J. Planning of sample size for wood anatomical investigations. Holz als Roh-und Werkstoff. 1987;45:141–144.

47. Oliver-Villanueva JV, Becker G. Verwendungsrelevante Holzeigenschaften der Esche (Fraxinus excelsior L.) und ihre Variabilitat im Hinblick auf Alter und Standraum. Forst und Holz. 1993;48:387–391.

48. Hapla F, Oliver-Villanueva JV, Gonzalez-Molina JM. Effect of silvicultural management on wood quality and timber utilisation of Cedrus atlantica in the European Mediterranean area. Holz als Roh-und Werkstoff. 2000;58(1–2):1–8. doi:10.1007/s001070050377.

49. Seeling U, Sachsse H (1991). Abnorme Kernbildung bei Rotbuche und ihr Einfluß auf holzbiologische und holztechnologische Kenngrößen [Abnormal heartwood formation in beech and its influence on the biological and technological features of the wood] (Doctoral dissertation, Doctoral thesis, 2nd).

50. Sauter U. Technologische Holzeigenschaften der Douglasie (Pseudotsuga menziesii (Mirb.) Franco) als Auspragung unterschiedlicher Wachstumsbedingungen. Freiburg i. Breisgau, Germany, 1992.

51. Dix B, Roffael E, Becker G, Gruss K. Properties of pulps prepared from poplar wood of different clones, sites and ages. Papier. 1992;46:583–592.

52. Wobst J (1995). Auswirkungen von Standortwahl und Durchforstungsstrategie auf verwertungsrelvante Holzeigenschaften der Douglasie (Pseudotsuga menziesii (Mirb. (Franco)) (Doctoral dissertation). UNIVERSITY OF GOTTINGEN.

53. Peters S (1996). Untersuchungen über die Holzeigenschaften der Stieleiche (Quercus robur L.) und ihre Beeinflussung durch die Bestandesdichte. Papierflieger, UNIVERSITY OF GOTTINGEN.

54. Restrepo, L. F., & González, J. (2007). From pearson to Spearman. Revista Colombiana de Ciencias Pecuarias, 20(2), 183-192.

55. Faraway, J. J. (2016). Extending the linear model with R: generalized linear, mixed effects and nonparametric regression models. CRC press.

56. Koppán, András, László Szarka, and Viktor Wesztergom. "Annual fluctuation in amplitudes of daily variations of electrical signals measured in the trunk of a standing tree." Comptes Rendus de l'Académie des Sciences-Series III-Sciences de La Vie 323.6 (2000): 559-563.

57. Le Mouël, J. L., Gibert, D., & Poirier, J. P. (2010). On transient electric potential variations in a standing tree and atmospheric electricity. Comptes Rendus Geoscience, 342(2), 95-99.

58. Observatorio Astronómico Nacional, Instituto Geográfico Nacional, Ministerio de Fomento, España. URL:https://astronomia.ign.es/web/guest/hora-salidas-y-puestas-de-sol. Access Date: December 15, 2020.

59. Belda-Palazón, B., Adamo, M., Valerio, C., Ferreira, L. J., Confraria, A., Reis-Barata, D., ... & Baena-González, E. (2020). A dual function of SnRK2 kinases in the regulation of SnRK1 and plant growth. Nature Plants, 1-9.

60. Matamoros, M. R., Merino, E. G., Ibáñez, N. I., & Bernal, E. M. (2008). Sensibilidad y grado de adaptación de" Pinus halepensis" mill. a la variabilidad climática en la provincia de Zaragoza. Cuadernos de la Sociedad Española de Ciencias Forestales, (26), 137-142.

61. Carriere, S. D., Ruffault, J., Pimont, F., Doussan, C., Simioni, G., Chalikakis, K., ... & Davi, H. (2020). Impact of local soil and subsoil conditions on inter-individual variations in tree responses to drought: insights from Electrical Resistivity Tomography. Science of the Total Environment, 698, 134247.

62. Cailleret, M., Nourtier, M., Amm, A., Durand-Gillmann, M., & Davi, H. (2014). Drought-induced decline and mortality of silver fir differ among three sites in Southern France. Annals of Forest Science, 71(6), 643-657.

63. Cailleret, M., Jansen, S., Robert, E. M., Desoto, L., Aakala, T., Antos, J. A., ... & Čada, V. (2017). A synthesis of radial growth patterns preceding tree mortality. Global change biology, 23(4), 1675-1690.

The ITACA-WIICT is a meeting forum for scientifics, technicians and other professionals who are dedicated to Information and communication technologies study and research. Its fundamental scope is to promote the contact among scientific and professionals, improving the cooperation as well as the technological transfer among professionals.

Institute ITACA
Information and Communication Technologies

978-84-09-46075-5